Experimental and Theoretical Studies of Vanadium Sulfide Cation

Ilona Kretzschmar, Detlef Schröder,* and Helmut Schwarz

Institut für Organische Chemie der Technischen Universität Berlin, Strasse des 17. Juni 135, D-10623 Berlin, Germany

Chad Rue and P. B. Armentrout*

Department of Chemistry, University of Utah, Salt Lake City, Utah 84112

Received: May 12, 1998; In Final Form: September 23, 1998

The reactions of V^+ (^5D) with CS_2 and COS and the reactions of VS^+ with Xe, CO, COS, CO_2, and D_2 are studied as a function of translational energy in a guided-ion-beam (GIB) mass spectrometer. From these experiments, $D_0(V^+-S) = 3.78 \pm 0.10$ eV, $D_0(V^+-CS) = 1.70 \pm 0.08$ eV, and $D_0(V^+-SD) = 2.57 \pm 0.15$ eV are derived. Verification of $D_0(V^+-S)$ is achieved by probing reactions of V^+ and VS^+ in a Fourier transform ion cyclotron resonance mass spectrometer. The good agreement between the thermochemistry obtained in the V^+/CS_2 system and that from the other systems studied shows that the formally spin-forbidden formation of ground-state VS^+ ($^3\Sigma^-$) from V^+ (^5D) and CS_2 has no activation barrier in excess of the reaction endothermicity. At higher energies, the spin-allowed formation of VS^+ ($^5\Pi$) competes efficiently, giving rise to a composite shape of the VS^+ cross section. The adiabatic and vertical splittings between the $^3\Sigma^-$ and $^5\Pi$ states of VS^+ are calculated as 1.37 and 1.87 eV at the MR-ACPF level of theory. These values agree well with the splittings obtained in GIB and sector-field mass spectrometric experiments.

Introduction

Chemical transformations of sulfur compounds are widespread in biological, atmospheric, and geochemical environments and involve a large variety of reactions, many of which are formal oxidation−reduction processes.[1] Most of these oxidations are catalyzed by transition metals and involve the formation of S−S and S−O bonds. Transition metal sulfides play a particular role in biochemistry in that heterometallic sulfur complexes[2] form the active sites in several metalloenzymes.[3,4] In this respect, vanadium-containing heterometallic sulfur complexes have attracted immense interest in the past few years.[5,6] Further, mixed transition metal oxides and sulfides are used as versatile catalysts in several chemical and petrochemical processes.[4] While the sulfides exhibit less catalytic reactivity than their corresponding oxides or bare metals, they are often less susceptible to poisoning and can show higher selectivity.[7]

A first step toward an understanding of the chemistry involved at a molecular level is to investigate the intrinsic properties of isolated metal oxides and sulfides, i.e., to conduct gas-phase experiments. In fact, several mass spectrometric methods have proven to be useful for this purpose and have been applied to numerous transition metal compounds in the past decade.[8,9] For example, the reactivity and thermochemistry of the diatomic transition metal oxide ions have been studied comprehensively.[9,10] However, despite their enormous relevance in biochemistry, the gas-phase chemistry of transition metal sulfides has been examined sparsely to date.[11,12]

In this work, we present a combined experimental and theoretical study of vanadium sulfide cation. To this end, three different mass spectrometric techniques have been used and the experiments are complemented by high-level ab initio studies. In addition, the ground- and excited-state properties of the vanadium sulfide cation are compared to those of its lighter congener VO^+.

Experimental and Computational Methods

Three different types of experiments have been performed: (i) thermochemical data for VS^+ were assessed by threshold collision-induced dissociation (CID) and ion/molecule reactions at elevated kinetic energies using a guided ion beam (GIB) apparatus; (ii) rate constants of exothermic reactions were obtained by Fourier transform ion cyclotron resonance (FTICR) mass spectrometry; (iii) excited states of VS^+ were investigated by high-resolution translational energy loss spectroscopy (HR-TELS) using a sector mass spectrometer (sector-MS). Only a brief description of these techniques is given here as the experimental details have been described in detail in previous publications.[13−16]

GIB. The guided ion beam apparatus used in this study and the data reduction procedures have been outlined earlier.[13,14] Ar^+ ions are created in a dc discharge and accelerated toward a vanadium cathode, thus sputtering off V^+ ions. These ions drift in a meter-long flow tube containing a 9:1 mixture of helium and argon at pressures of 0.7 Torr. VS^+ ions are formed by introducing carbonyl sulfide as a sulfur-transfer reagent ca. 60 cm downstream from the dc discharge. The ions undergo 10^5 collisions with the buffer gas before exiting the flow tube, and therefore are expected to have equilibrated to a temperature of 300 K with respect to vibrational and rotational states. Because helium does not always effectively quench excited electronic states of transition metals,[17] methane is introduced ca. 10 cm downstream from the discharge at pressures between

* Authors to whom correspondence should be addressed.

10.1021/jp982199w CCC: $15.00
Published on Web 11/11/1998

0.5 and 4 mTorr such that the ions undergo 10^2-10^3 collisions with methane. Excited vanadium ions in the a^3F as well as higher electronic states react rapidly with CH_4,[18] which effectively removes these ions from the flow tube. However, the lowest-lying excited state of V^+ is an a^5F state ($\Delta E = 0.32$ eV)[19] with a $3d^34s^1$ configuration, which is not reactive toward methane.[18] A detailed analysis of the contribution of the a^5F state to the cross sections observed in the reaction of V^+ with CS_2 is given elsewhere.[20]

The ions are extracted from the source, accelerated, and focused into a magnetic sector. Mass-selected ions are decelerated to a desired kinetic energy and focused into an octopole ion trap.[13] This device guides the ions through a static gas cell (8.26 cm effective length) which is kept at a sufficiently low pressure (0.05−0.1 mTorr) of the reactant gas that multiple collisions are improbable. The assumption of single-collision conditions is verified by examining the pressure dependence of the product intensities. After exiting the gas cell, product and unreacted beam ions drift to the end of the octopole where they are directed into a quadrupole mass filter for mass analysis and detected. Conversion of the raw ion intensities into reaction cross sections and the calibration of the absolute energy scale are treated as described previously.[13] The accuracy of the absolute cross sections is estimated to be 20%. The beams have Gaussian kinetic energy distributions with an average full width at half-maximum (fwhm) of ca. 0.27 eV in the laboratory frame. The uncertainty of the absolute energy scale is 0.05 eV (lab).

Quantitative analysis of the energy dependence of these cross sections is achieved using eq 1 and methods outlined elsewhere:[21]

$$\sigma(E) = \sigma_0 \Sigma g_i (E + E_i - E_0)^n / E^m \qquad (1)$$

In eq 1, E is the relative kinetic energy of reactants, E_0 is the threshold for reaction at 0 K, σ_0 is a scaling parameter, and n and m are fitting parameters where $m = 1$ in all but unusual circumstances. The summation is over the rovibrational states of the reactants having energies E_i and populations g_i ($\Sigma g_i = 1$). The vibrational frequencies of the neutral reagents are taken from the literature.[22] The vibrational frequency for VS^+ is calculated at the B3LYP/6-311+G* level of theory as 532 cm^{-1}. This model is compared to the data after convoluting with the kinetic energy distributions of the reactants. The σ_0, n, and E_0 parameters are optimized to best reproduce the data using a least-squares criterion. Reported uncertainties in E_0 reflect the range of values obtained for several data sets and the absolute uncertainty in the energy scale.

Equation 1 is expected to be appropriate for translationally driven reactions.[23] This model form has been found to reproduce reaction cross sections well in a number of previous studies of both atom−diatom and polyatomic reactions,[21,24] including CID processes.[25] Equation 1 explicitly includes the internal energy of the reactants and makes the statistical assumption that all of the internal energy is capable of coupling into the reaction coordinate. This is the most reasonable assumption in the absence of specific information concerning state-specific dynamic effects. Thus, the threshold for product formation corresponds to the formation of products with no internal excitation, and therefore corresponds to the threshold at 0 K. These assumptions have been shown to lead to accurate thermochemistry in several previous studies.[21,25,26]

FTICR. The experiments are performed in a Spectrospin-CMS-47X Fourier transform ion-cyclotron resonance mass spectrometer equipped with an external ion source.[15] Briefly, V^+ ions are generated via laser desorption/laser ionization by focusing the beam of a Nd:YAG laser (Spectron Systems, $\lambda =$ 1064 nm) onto a vanadium target. The ions are extracted from the source and transferred into the analyzer cell by a system of electrostatic potentials and lenses. After deceleration, the ions are trapped in the field of a superconducting magnet (maximum field strength 7.05 T). The most abundant isotope $^{51}V^+$ is mass-selected from the other isotope using FERETS,[27] a computer-assisted protocol that combines frequency sweeps and single-frequency ion-ejection pulses to optimize ion isolation. Generation of the VX^+ ions (X = O, S) is achieved using either molecular oxygen or carbonyl sulfide, respectively, as reagent gases for X transfer. Then, the ions under investigation are again isolated using FERETS. In general, the ions are collided with pulsed-in methane (2000 collisions) for thermalization and removal of excess energy. The kinetics of all reactions are carefully studied as a function of thermalizing collisions in order to ensure that the ions undergoing ion/molecule reactions are not kinetically or electronically excited. The reactants are admitted to the cell through leak valves at stationary pressures between 0.08 and 0.8 Torr (as measured by a Balzers IMG070 ion gauge).

Sector-MS. The HRTELS experiments[28] are performed in the first two sectors of a four-sector tandem mass spectrometer of BEBE configuration (B stands for magnetic and *E* for electric sector).[16] The VS^+ ions are generated by chemical ionization of a mixture of VOF_3 and CS_2. The VO^+ ions are obtained by electron ionization of VOF_3. Briefly, VX^+ (X = O, S) ions of 8 keV translational energy are mass-selected by B(1) and focused into a collision cell where oxygen is admitted as a collision gas; the pressure is adjusted to yield 20% ion transmission. Translational energy analysis of the beam profile is accomplished by scanning the electric sector. In the absence of the collision gas, the energy resolution of the VX^+ beam is ca. 0.5 eV (fwhm). During the interaction of the collision gas and the 8 keV VX^+ ions, the energies of the ions may be altered due to excitation of ground states or de-excitation of excited states. The former event results in peaks at lower and the latter in signals at higher translational energies as compared to the kinetic energy of the unscattered beam. The experiment is designed to record only those collisions occurring at small scattering angles. Consequently, translational energy changes of the ion correspond to changes in the ion's internal energy.[28] Because these collisions involve rather short time scales ($<10^{-14}$ s), the HRTELS experiments sample vertical excitations.

Calculations. The bond lengths and the ground-state/excited-state splitting of VX^+ (X = O, S) are calculated with density functional theory (DFT). The DFT calculations are carried out using the Amsterdam density functional (ADF, version 2.0.1) suite of programs[29] with the inner-shell electrons ([He] for O, [Ne] for S, and [Ar] for V) treated in the frozen-core approximation.[30] The valence orbitals are expanded as linear combinations of Slater-type basis functions. Triple-ζ basis sets are used for vanadium, oxygen, and sulfur. All molecular and atomic energies are calculated using the local spin-density approximation (LDA) with Slater's exchange functional and the Vosko−Wilk−Nusair parametrization (VWN)[31] augmented by Becke's[32] and Perdew's[33] (BP) gradient corrections for the exchange and correlation potential, respectively.[34] This method will be referred to as ADF/BP. A particular advantage of the ADF program is that it (i) provides control over the symmetry of the wave function created during geometry optimizations and (ii) permits the calculations of the excited states.

TABLE 1: Basis Sets I−IV

	vanadium	sulfur	oxygen
BS I	(8s7p6d1f)/[6s5p3d1f][a]	(13s9p2d)[5s4p2d]	(10s5p2d)[4s4p2d]
BS II	(21s15p10d6f)/[6s5p4d2f]	(17s12p5d)[7s6p4d]	(14s9p4d)[6s5p3d]
BS III	(21s15p10d6f4g)/[8s7p5d3f2g]	(17s12p5d4f)[7s6p4d3f]	(14s9p4d3f)[6s5p3d2f]
BS IV	(21s15p10d6f4g1h)/[8s7p5d3f2g1h]	(17s12p5d4f1g)[7s6p4d3f1g]	

[a] Ten core electrons of vanadium ($1s^2 2s^2 2p^6$) were treated with a relativistic electron−core potential as described by Dolg et al.[38]

For the ground-state VS^+ ($^3\Sigma^-$), the bond length obtained with ADF is re-optimized using the multi-configuration self-consistent field[35] (MCSCF) and internally contracted multireference averaged coupled-pair functional[36] (MR-ACPF) methods as implemented in the MOLPRO96[37] program. Because there are only minor changes upon switching between the different levels of theory (<0.04 Å, < 0.01 eV), the bond lengths obtained with ADF are used for both the MCSCF and MR-ACPF calculations. The active space in the calculations includes the 3d- and 4s-orbitals of vanadium, the 2p-orbitals of oxygen, and the 3p-orbitals of sulfur. The 2s- and 3s-orbitals of oxygen and sulfur, respectively, are not included because of a mixing of the s-orbitals with the inner-shell $3p_z$-orbital of vanadium (see below). Further, the state splitting for VX^+ is evaluated at the MCSCF and MR-ACPF levels of theory using the ADF optimized geometries. The MR-ACPF method is considered more reliable than MCSCF because it also includes dynamic correlation.

Basis set I (Table 1) uses a quasirelativistic ab initio pseudopotential[38] for the 10 core electrons of vanadium and describes the remaining 3s, 3p, and 3d electrons with a (8s7p6d1f)/[6s5p3d1f] contracted basis set. For sulfur, the standard augmented correlation-consistent polarized valence double-ζ basis set of Dunning[39] (aug-cc-pVDZ) is used. Basis sets II−IV are derived from the generally contracted atomic natural orbital (ANO)[40] all-electron basis sets of Roos for vanadium,[41] oxygen, and sulfur,[42] respectively. The number of *f* and *g* functions increases going from BS II to BS III, and additional polarization functions, i.e., an *h* function on vanadium ($\alpha = 0.872$) and a *g* function on sulfur ($\alpha = 0.683$),[43] are added in BS IV. All computations are performed on either IBM/RS 6000 workstations or a CRAY−YMP computer. If not stated otherwise, the values given in the text for VS^+ refer to the MR-ACPF level of theory using BS IV, while the results for VO^+ are obtained with BS III. Vibrational frequencies of VO^+ (1141 cm^{-1}), VS^+ (532 cm^{-1}), and S_2 (685 cm^{-1}) are calculated with the B3LYP/6-311+G* approach and used for zero-point vibrational energy (ZPVE) correction. Contributions of spin−orbit coupling (SOC) are neglected in the calculations.

Results

A. Experimental Results. Three different mass spectrometric techniques are employed to examine the energetics of VS^+. First, VS^+ is formed in ion−molecule reactions of V^+ at thermal or hyperthermal energies mainly using the GIB technique. Second, ion−molecule reactions of VS^+ that yield previously characterized products are used to derive additional thermochemical and kinetic information. Finally, electronic excitation of VX^+ (X = O, S) is examined in high-energy collisions with molecular oxygen. Whenever possible, reaction energies at 0 K are calculated from the thermodynamic values in Tables 2 and 3 and are shown next to reaction equations in square brackets. In general, these calculations utilize bond energies rather than heats of formation, as use of the latter propagates the correlated uncertainty in $\Delta_f H°(V^+)$. Exceptions include the values listed below for reactions 5 and 6, which are based on heats of formation for the neutral species, that for reaction 3, which is determined in ref 20, and those for reactions 17, 20, and 25, which are determined here. Following the standard convention, positive numbers refer to endothermic processes and negative numbers refer to exothermic processes.

TABLE 2: Heats of Formation and Bond Dissociation Energies for Ionic Species at 0 K

ionic species	$\Delta_f H°$ [eV]	bond	D_0 [eV]
V^+	12.05 (0.08)[a]		
VD^+	12.24 (0.10)[b]	V^+−D	2.09 (0.06)[b]
VC^+	15.46 (0.09)[c]	V^+−C	3.96 (0.04)[c]
VO^+	8.62 (0.13)[d]	V^+−O	5.99 (0.10)[d]
VS^+	11.12 (0.13)[e]	V^+−S	3.78 (0.10)[e]
VSD^+	10.91 (0.16)[e]	VS^+−D	2.49 (0.10)[e]
		V^+−SD	2.57 (0.15)[e]
VCS^+	13.20 (0.12)[f]	V^+−CS	1.70 (0.08)[f]
VOS^+	10.11 (0.21)[e]	SV^+−O	3.57 (0.17)[e]
		OV^+−S	1.36 (0.22)[e]
VCO^+	9.70 (0.09)[g]	V^+−CO	1.17 (0.03)[g]
VCO_2^+	7.23 (0.09)[h]	V^+−CO_2	0.75 (0.04)[h]
VS_2^+	≤10.82 (0.13)[e]	SV^+−S	≥3.14 (0.005)[e]

[a] Chase, M. W., Jr.; Davies, C. A.; Downey, J. R., Jr.; Frurip, D. J.; McDonald, R. A.; Syverud, A. N. *J. Phys. Chem. Ref. Data* **1985**, *14*, Suppl. 1 (JANAF Tables). [b] Ref 65. [c] Aristov, N.; Armentrout, P. B. *J. Am. Chem. Soc*. **1986**, *108*, 1806. ref 17b. [d] Ref 59. [e] This work. [f] Ref 20. [g] Ref 62. [h] Ref 44.

TABLE 3: Heats of Formation and Bond Dissociation Energies for Neutral Species at 0 K[a]

neutral species	$\Delta_f H°$ [eV]	bond	D_0 [eV]
C	7.371 (0.005)		
S	2.847 (0.003)		
H	2.239	H−H	4.478
D	2.278	D−D	4.556
O	2.558 (0.001)	O−O	5.116 (0.001)
CO	−1.180 (0.002)	C−O	11.109 (0.005)
SD	1.43 (0.05)	S−D	3.70 (0.05)
CS	2.85 (0.04)[b]	C−S	7.37 (0.04)
SO	0.052 (0.013)	S−O	5.353 (0.013)
S_2	1.330 (0.003)	S−S	4.364 (0.005)
CS_2	1.200 (0.008)[c]	SC−S	4.50 (0.04)
COS	−1.473 (0.003)[c]	OC−S	3.140 (0.005)
		SC−O	6.88 (0.04)
CO_2	−4.075 (0.001)	OC−O	5.453 (0.002)
H_2O	−2.476 (0.0004)	O−H_2	5.034 (0.001)
H_2S	−0.182 (0.008)	S−H_2	3.029 (0.009)
D_2S	−0.218 (0.008)	S−D_2	3.065 (0.009)
		DS−D	3.93 (0.05)

[a] Chase, M. W., Jr.; Davies, C. A.; Downey, J. R., Jr.; Frurip, D. J.; McDonald, R. A.; Syverud, A. N. *J. Phys. Chem. Ref. Data* **1985**, *14*, Suppl. 1 (JANAF Tables). [b] Prinslow, D. A.; Armentrout, P. B. *J. Chem. Phys*. **1991**, *94*, 3563. [c] Pedley, J. B.; Naylor, R. D.; Kirby, S. P. *Thermochemical Data of Organic Compounds*; Chapman and Hall: London, 1986. Corrected to 0 Kelvin using $H°-H°$ (298.15) values taken from the reference in footnote *a*.

Reaction of V^+ with CS_2. In the GIB mass spectrometer, vanadium cation reacts with CS_2 by two major pathways, reactions 2 and 3. Other products, VC^+, CS_2^+, and VS_2^+, are also observed in minor quantities, but the cross sections are very small (magnitudes below 0.02×10^{-16} cm^2) and not discussed any further. The cross sections obtained for the two

TABLE 4: Summary of Parameters in Eq 1 Used for the Fits of the Cross Sections and the Derived $D_0(V^+-S)$

reaction	reaction no.	E_0 [eV][a]	σ_0	n	$D_0(V^+-S)$ [eV]
$V^+ + CS_2 \rightarrow VS^+ + CS$	(2)	0.78 (0.08)	7.39 (1.42)	0.5 (0.1)	3.72 (0.09)
$\rightarrow VCS^+ + S$	(3)	2.80 (0.07)	1.51 (0.33)	1.8 (0.2)	
$V^+ + COS \rightarrow VS^+ + CO$	(7)	<0			>3.14 (0.01)
$\rightarrow VCO^+ + S$	(9)	2.30 (0.09)	1.31 (0.19)	1.3 (0.3)	
$VS^+ + Xe \rightarrow V^+ + S + Xe$	(11)	4.14 (0.17)	0.90 (0.35)	2.3 (0.1)	<4.14 (0.17)
$VS^+ + CO \rightarrow V^+ + COS$	(12)	0.88 (0.40)	0.02 (0.01)	2.4 (0.2)	4.02 (0.40)
$\rightarrow VO^+ + CS$	(13)	2.96 (0.48)	0.11 (0.02)	1.9 (0.3)	5.21 (0.49)
		4.39 (0.10)	0.33 (0.16)	1.9 (0.2)	
$\rightarrow V^+ + S + CO$	(14)				<4.59 (0.30)
		4.79 (0.10)	0.94 (0.14)	1.8 (0.2)	
$VS^+ + CO_2 \rightarrow VOS^+ + CO$	(17)	1.88 (0.17)	0.04 (0.02)	1.6 (0.3)	
$\rightarrow V^+ + S + CO_2$	(19)	5.03 (0.30)	1.45 (0.30)	1.4 (0.2)	<5.03 (0.30)
$VS^+ + COS \rightarrow V^+ + S_2 + CO$	(21)	2.42 (0.18)	1.34 (0.15)	1.7 (0.2)	3.64 (0.18)
$\rightarrow VO^+ + CS + S$	(23)	4.56 (0.48)	0.15 (0.04)	1.7 (0.2)	3.67 (0.49)
$VS^+ + D_2 \rightarrow V^+ + D_2S$	(24)	0.79 (0.08)	0.12 (0.02)	1.3 (0.2)	3.85 (0.08)
$\rightarrow VSD^+ + D$	(25)	2.07 (0.10)	3.87 (0.71)	1.5 (0.3)	
$\rightarrow VD^+ + DS$	(26)	2.52 (0.13)	0.12 (0.03)	1.6 (0.3)	3.75 (0.15)

[a] The E_0 values are the average of several threshold fits with uncertainties of one standard deviation.

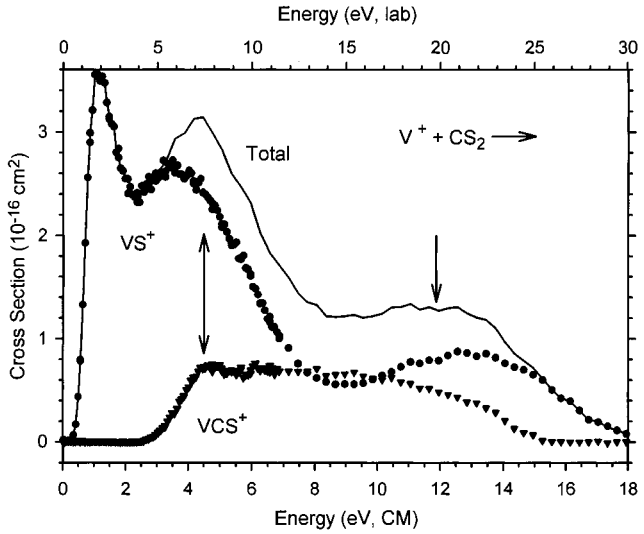

Figure 1. Product cross sections for the reaction of cooled (4 mTorr methane) V^+ with CS_2 to form VS^+ (●) and VCS^+ (▼) as a function of center of mass energy (lower axis) and laboratory energy (upper axis). The arrows mark the dissociation energies of CS_2 at 4.50 and 11.87 eV (see text).

major product channels are shown in Figure 1.

$$V^+ + CS_2 \rightarrow VS^+ + CS \qquad [0.72 \pm 0.11 \text{ eV}] \qquad (2)$$

$$\rightarrow VCS^+ + S \qquad [2.80 \pm 0.07 \text{ eV}] \qquad (3)$$

In contrast to the reaction of V^+ and CO_2, in which the formation of VO^+ in its $^3\Sigma^-$ ground state is exothermic,[44] sulfur transfer is endothermic for the V^+/CS_2 couple. Nevertheless, reaction 2 dominates over the whole energy range considered, and its cross section exhibits three endothermic features between 0 and 18 eV center-of-mass energy (Figure 1). The VS^+ cross section rises rapidly from an apparent threshold of 0.4 eV to reach a maximum near 1 eV. Upon further increase of the collision energy, the cross section drops by about one-third before it rises near 2 eV and peaks again at ca. 3.5 eV. As there are no alternative pathways for production of VS^+ in this energy range, both features must be assigned to reaction 2. The competitive formation of VCS^+ in reaction 3 leads to a decrease of the VS^+ cross section starting near 3.5 eV, while the sum of both cross sections (σ_{total}) still increases (Figure 1). At about 4.5 eV of kinetic energy, reaction 4, corresponding to dissociation of either VS^+ or VCS^+ product ions, becomes feasible and σ_{total} decreases at higher energies:

$$V^+ + CS_2 \rightarrow V^+ + S + CS \qquad [4.50 \pm 0.04 \text{ eV}] \qquad (4)$$

The VS^+ cross section exhibits a third, high-energy feature with a broad maximum near 12 eV. After models (eq 1) for the low-energy features are subtracted from the data, we obtain a threshold on the order of 8 eV for this third feature. This value is in good agreement with the thermochemistry of reaction 5 (Tables 2 and 3). The decrease of the total cross section above 12 eV can be attributed to complete dissociation according to reaction 6:

$$V^+ + CS_2 \rightarrow VS^+ + C + S \qquad [8.09 \pm 0.10 \text{ eV}] \qquad (5)$$

$$V^+ + CS_2 \rightarrow V^+ + C + 2S \qquad [11.87 \pm 0.01 \text{ eV}] \qquad (6)$$

The second major process observed is the formation of VCS^+. Analysis of this cross section[20] yields a threshold of 2.80 ± 0.07 eV (Table 4). The cross section reaches its maximum near $D_0(SC-S)$, thus indicating that the abrupt change in slope above 4.5 eV is also due to reaction 4, dissociation of the VCS^+ product to V^+ and CS.

Reaction of V^+ with COS. The cross sections observed for the reaction of V^+ with COS are shown in Figure 2 and correspond to reactions 7−9:

$$V^+ + COS \rightarrow VS^+ + CO \qquad [-0.64 \pm 0.10 \text{ eV}] \qquad (7)$$

$$\rightarrow VO^+ + CS \qquad [0.89 \pm 0.11 \text{ eV}] \qquad (8)$$

$$\rightarrow VCO^+ + S \qquad [1.97 \pm 0.03 \text{ eV}] \qquad (9)$$

The cross section for VS^+ formation in process 7 increases with decreasing energy, which is indicative of an exothermic process ($\sigma_{max} = 183 \times 10^{-16}$ cm^2 at $E_{CM} = 0.02$ eV). Interestingly, the VS^+ cross section also exhibits an endothermic second feature which suggests that VS^+ is being formed by a second pathway at higher energies. By subtracting the exothermic feature from the cross section (modeled as $E^{-1.0}$), an estimate of the shape and threshold of the second feature may be obtained. Analysis of the feature with eq 1 yields $E_0 = 0.8 \pm 0.1$ eV. The cross section for VO^+ formed in reaction 8 is quite small over the wide energy range examined, making an accurate determination of E_0 difficult. However, it is straightforward to reproduce the observed cross section using eq 1 and

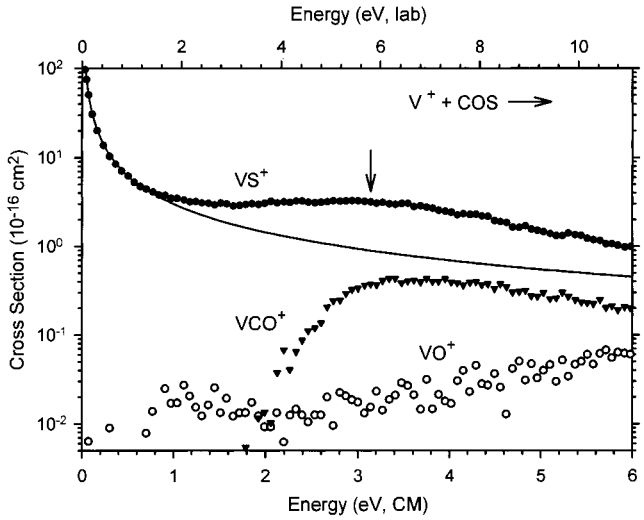

Figure 2. Product cross sections for the reaction of cooled (4 mTorr methane) V^+ with COS to form VO^+ (○), VCO^+ (▼), and VS^+ (●) as a function of center-of-mass energy (lower axis) and laboratory energy (upper axis). The solid line declines as $E^{-1.0}$. The arrow marks the S−CO bond energy at 3.14 eV.

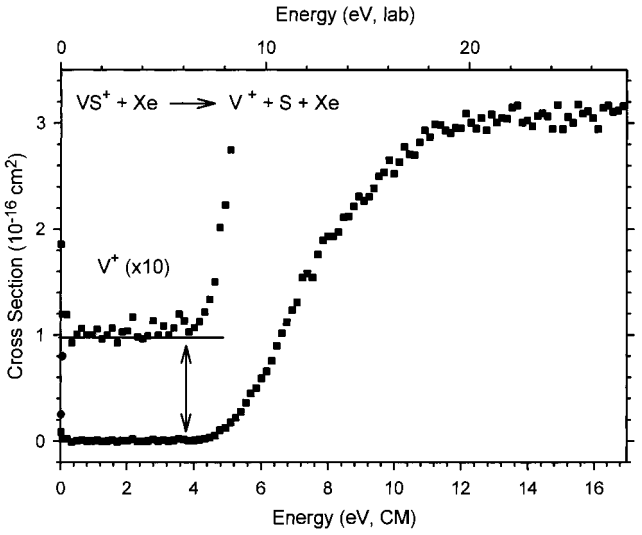

Figure 3. Cross section for the CID process of VS^+ with xenon to form V^+ (■) as a function of center-of-mass energy (lower axis) and laboratory energy (upper axis). The inset shows the threshold region of the V^+ cross section on an expanded vertical scale and offset from zero by 1×10^{-16} cm^2. The arrow marks the dissociation energy of VS^+ at 3.78 eV.

the calculated E_0 of 0.89 eV for reaction 8. The second main product formed in the V^+/COS system is VCO^+, formed in reaction 9. Analysis of the VCO^+ cross section yields a threshold of 2.30 ± 0.09 eV (Table 4). The slightly elevated threshold for formation of VCO^+ can be attributed to the strong competition with the formation of VS^+. Both the VS^+ and the VCO^+ cross sections decline above 3.1 eV, as dissociation of the ionic products in reaction 10 becomes possible:

$$V^+ + COS \rightarrow V^+ + CO + S \qquad [3.14 \pm 0.01 \text{ eV}] \qquad (10)$$

The formation of VC^+ is also observed in this system. It has a small cross section ($<0.05 \times 10^{-16}$ cm^2) and is not shown here for clarity.

Reactions of VS^+ with Xe, CO, CO_2, COS, and D_2. In this section, the reactions of VS^+ with several neutral target molecules will be described. VS^+ was generated in the flow tube of the GIB apparatus by reacting V^+ with COS. A possible interference may arise from metal dioxide cations which could be formed efficiently by exothermic reactions of the early transition metal cations M^+ (M = Sc, Ti, and V) with residual oxygen compounds.[45] While VO^+ cations are removed from the VS^+ ion beam by mass selection, the dioxide cations are isobaric with VS^+ and cannot be resolved using a single magnetic sector. It is straightforward to check for VO_2^+ impurities in the VS^+ beam by performing CID of the mass selected ionic reactant with xenon. The diatomic VS^+ molecule must dissociate to give V^+, while CID of VO_2^+ yields almost exclusively VO^+.[46] The only significant product observed in the CID of our VS^+ beam was V^+ (maximum cross section of 3×10^{-16} cm^2), with only trace amounts of VO^+ detected (maximum cross section of less than 0.01×10^{-16} cm^2). Thus, we conclude that there is no significant amount of VO_2^+ in the reactant ion beam (<1%) used for the GIB study of the reactions discussed below.

The cross section for the interaction of neutral Xe with VS^+ ions is depicted in Figure 3. The only process observed corresponds to dissociation according to reaction 11:

$$VS^+ + Xe \rightarrow V^+ + S + Xe \qquad [3.78 \pm 0.10 \text{ eV}] \qquad (11)$$

Analysis of the CID cross section with eq 1 yields a threshold of 4.14 ± 0.17 eV (Table 4), somewhat larger than the thermochemical threshold of 3.78 eV. The origin of this discrepancy is discussed below.

In the interaction of VS^+ with CO, three product channels are observed and correspond to reactions 12−15:

$$VS^+ + CO \rightarrow V^+ + COS \qquad [0.64 \pm 0.10 \text{ eV}] \qquad (12)$$

$$\rightarrow VO^+ + CS \qquad [1.53 \pm 0.15 \text{ eV}] \qquad (13)$$

$$\rightarrow V^+ + S + CO \qquad [3.78 \pm 0.10 \text{ eV}] \qquad (14)$$

$$\rightarrow VC^+ + S + O \qquad [10.93 \pm 0.11 \text{ eV}] \qquad (15)$$

The measured cross sections (Figure 4) demonstrate that all processes are endothermic. Formation of V^+ dominates and corresponds primarily to the CID of VS^+, reaction 14, a result fully in line with the strong CO bond, $D_0(C-O) = 11.109 \pm 0.005$ eV, which needs to be broken in reactions 13 and 15. However, careful inspection of the V^+ channel reveals that the cross section has a threshold well below the 3.78 eV expected for the CID process 14, indicating that another process is involved in the formation of V^+ at lower energies. The only process which has a threshold near 1 eV corresponds to the cleavage of the V−S bond concomitant with formation of carbonyl sulfide according to reaction 12, the reverse of reaction 7. Analysis of the low-energy feature of the V^+ cross section with eq 1 yields a threshold of 0.88 ± 0.40 eV (Table 4), which is consistent with the assignment of reaction 12 to the low-energy feature.

The threshold for the CID process 14 can be obtained by subtracting the small feature attributed to reaction 12 from the V^+ cross section. Because the high-energy behavior of reaction 12 is unknown, a range for the CID threshold is established by considering two possible extremes. A lower limit of 4.39 ± 0.10 eV is derived by assuming that the cross section of process 12 declines above 3.78 eV, while an upper limit of 4.79 ± 0.10 eV is obtained assuming that there is no decline at energies higher than 3.78 eV (Table 4). These limits lead to an experimental threshold of 4.59 ± 0.30 eV for the CID reaction 14.

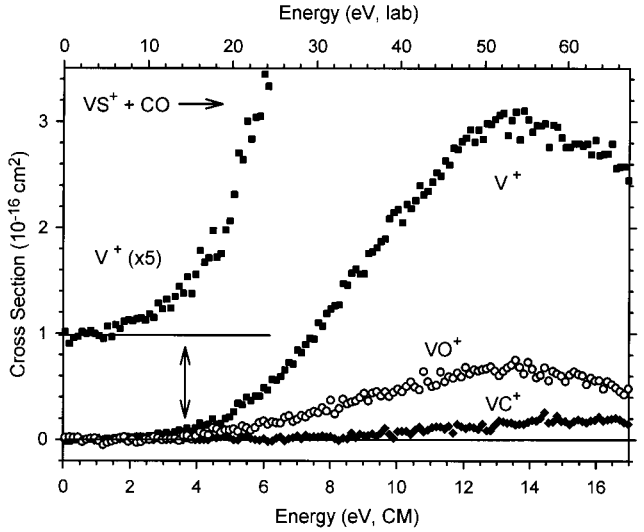

Figure 4. Product cross sections for the reaction of VS^+ and CO to form V^+ (■), VO^+ (○), and VC^+ (◆) as a function of center-of-mass energy (lower axis) and laboratory energy (upper axis). The inset shows the threshold region of the V^+ cross section on an expanded vertical scale and offset from zero by 1×10^{-16} cm^2. The low-energy part of the V^+ cross section is assigned to formation of $V^+ + COS$ (see text). The arrow marks the dissociation energy of VS^+ at 3.78 eV.

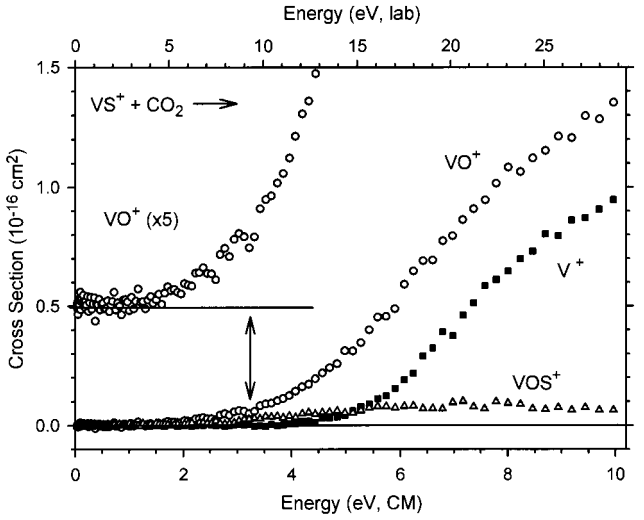

Figure 5. Product cross sections for the reaction of VS^+ and CO_2 to form VO^+ (○), V^+ (■), and VOS^+ (△) as a function of center-of-mass energy (lower axis) and laboratory energy (upper axis). The inset shows the threshold region of the VO^+ cross section on an expanded vertical scale and offset from zero by 0.5×10^{-16} cm^2. The low-energy part of the VO^+ cross section is assigned to formation of $VO^+ + COS$ (see text). The arrow marks the calculated threshold for formation of VO^+ according to reaction 18 at 3.24 eV.

The apparent threshold for the formation of VO^+ in reaction 13 is about 3 eV. This value is significantly higher than the calculated thermodynamic threshold of 1.53 ± 0.15 eV and suggests the presence of a barrier associated with the O/S metathesis in excess of the reaction endothermicity. The least efficient process observed in this system involves the formation of VC^+ according to reaction 15 with an apparent threshold near 9.5 eV. The cross section for process 15 is very small and will not be analyzed further.

Three product channels, formation of V^+, VO^+, and VOS^+, are observed in the energy-dependent cross sections for the reaction of VS^+ with neutral CO_2 (Figure 5):

$$VS^+ + CO_2 \rightarrow VO^+ + COS \quad [0.10 \pm 0.14 \text{ eV}] \quad (16)$$

$$\rightarrow VOS^+ + CO \quad [1.88 \pm 0.17 \text{ eV}] \quad (17)$$

$$\rightarrow VO^+ + S + CO \quad [3.24 \pm 0.14 \text{ eV}] \quad (18)$$

$$\rightarrow V^+ + S + CO_2 \quad [3.78 \pm 0.10 \text{ eV}] \quad (19)$$

In contrast to the VS^+/CO couple, VO^+ formation prevails in the VS^+/CO_2 system. This is a result of the much weaker C−O bond in CO_2 compared to CO (Table 3). Careful analysis of the threshold region for formation of VO^+ reveals the presence of a small endothermic feature at low energies, that can be assigned to the formation of COS in reaction 16.[47] Because the VO^+ cross section is so small, analysis of this channel is difficult and no meaningful thresholds can be derived for reactions 16 and 18; however, the measured VO^+ cross section can be reproduced using eq 1 and the thermodynamic thresholds.

The least efficient process in the reaction of VS^+ with CO_2 is the formation of the mixed dichalcogenide VOS^+, reaction 17. Analysis of the threshold using eq 1 leads to $E_0 = 1.88 \pm 0.17$ eV (Table 4) which leads to $D_0(SV^+-O) = 3.57 \pm 0.17$ eV. The CID process 19 has an apparent threshold near 4 eV, but analysis of the threshold region yields $E_0 = 5.03 \pm 0.30$ eV (Table 4), which is about 1 eV higher than the threshold obtained with xenon. It should be noted that this analysis fails to accurately reproduce data points in the threshold region (see below).

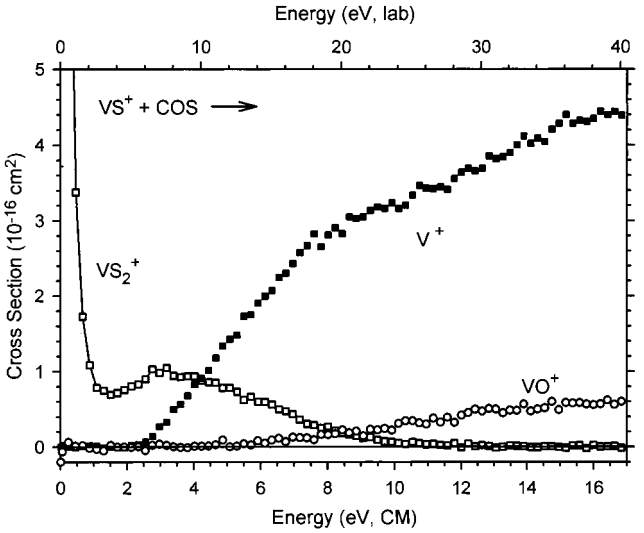

Figure 6. Product cross sections for the reaction of VS^+ and COS to form VS_2^+ (□), V^+ (■), and VO^+ (○) as a function of center-of-mass energy (lower axis) and laboratory energy (upper axis).

The product channels observed in the reaction of VS^+ with COS (Figure 6) are assigned to reactions 20−23. Both sulfur-atom transfer 20 and oxygen-atom transfer 23 occur:

$$VS^+ + COS \rightarrow VS_2^+ + CO \quad [<0 \text{ eV}] \quad (20)$$

$$\rightarrow V^+ + S_2 + CO \quad [2.56 \pm 0.10 \text{ eV}] \quad (21)$$

$$\rightarrow V^+ + S + COS \quad [3.78 \pm 0.10 \text{ eV}] \quad (22)$$

$$\rightarrow VO^+ + CS + S \quad [4.67 \pm 0.15 \text{ eV}] \quad (23)$$

The observation of an exothermic feature ($\sigma_{max} = 59 \times 10^{-16}$ cm^2 at $E_{CM} = 0.02$ eV) in the cross section for the formation of the disulfide implies that the carbon−sulfur bond in COS is

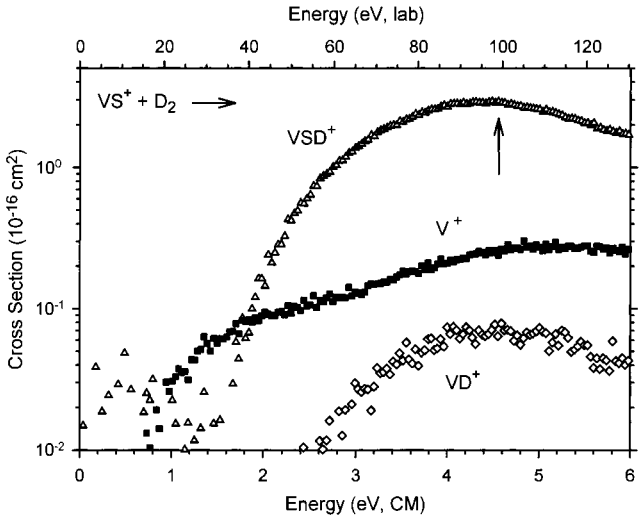

Figure 7. Product cross sections for the reaction of VS^+ and D_2 to form V^+ (■), VD^+ (◇), and VSD^+ (Δ) as a function of center-of-mass energy (lower axis) and laboratory energy (upper axis). The arrow marks the D_2 bond energy at 4.56 eV.

weaker than a vanadium−sulfur bond in VS_2^+, i.e., $D_0(SV^+-S) \geq D_0(OC-S) = 3.140 \pm 0.005$ eV. The endothermic feature in the VS_2^+ cross section, which begins near 1 eV, plausibly indicates the formation of electronically excited VS_2^+. Because VS_2^+ is believed to have a singlet ground state,[48] a likely assignment for such an excited state is a triplet as this makes reaction 20 spin-allowed. Interestingly, the V^+ channel has a threshold of 2.42 ± 0.18 eV (Table 4), far below the thresholds obtained for the CID of VS^+ with Xe, CO, and CO_2. This threshold is consistent with the endothermicity of reaction 21, formation of V^+ by loss of the CO and S_2 neutrals. The driving force for reaction 21 is the formation of the strong S−S bond, $D_0(S-S) = 4.364 \pm 0.005$ eV. This reaction assignment is further supported by the fact that the V^+ cross section has its threshold in the region where the endothermic feature of the VS_2^+ channel starts to decline. So, a possible mechanistic explanation is the formation of VS_2^+ at low energies, followed by loss of disulfur beginning near 2.5 eV.[49] The formation of VO^+ has a threshold measured to be 4.56 ± 0.48 eV (Table 4), in good agreement with the calculated threshold. This is the least efficient process in the reaction of VS^+ with COS, largely because of the strong C−O bond, $D_0(SC-O) = 6.88 \pm 0.04$ eV.

Figure 7 shows the cross sections for the reaction of D_2 with VS^+ in which two main products corresponding to reactions 24 and 25 are formed. These products are analogous to those formed in the reaction of D_2 with early transition metal oxide cations MO^+ (M = Sc, Ti, and V) where formation of metal hydroxide cations and bare M^+ is observed:[50]

$$VS^+ + D_2 \rightarrow V^+ + D_2S \qquad [0.71 \pm 0.10 \text{ eV}] \qquad (24)$$

$$\rightarrow VSD^+ + D \qquad [2.07 \pm 0.10 \text{ eV}] \qquad (25)$$

$$\rightarrow VD^+ + DS \qquad [2.55 \pm 0.13 \text{ eV}] \qquad (26)$$

$$\rightarrow V^+ + S + D_2 \qquad [3.78 \pm 0.10 \text{ eV}] \qquad (27)$$

The observed experimental threshold for the V^+ cross section is quite low, which rules out formation of V^+ by simple CID, reaction 27. Analysis of the cross section (Table 4) yields a threshold of 0.79 ± 0.08 eV, in good agreement with the calculated onset for reaction 24. The shape of the V^+ cross section is influenced by the competitive formation of VSD^+, which causes a change in the slope of the V^+ cross section near 1.8 eV (Figure 7). Above this energy, the V^+ cross section rises more slowly before increasing again near 3.3 eV (more obvious when plotted on a linear scale). This behavior suggests that there is at least one more process contributing to the V^+ cross section at higher energies. Two possibilities are (i) simple CID of VS^+, reaction 27, which requires at least 3.78 eV, and (ii) the formation of V^+ in excited electronic states. Given that VS^+ has a $^3\Sigma^-$ ground state (see Theoretical Results), a possible process is the spin-allowed formation of V^+ in the lowest-lying triplet state, a^3F, which has a threshold of 1.81 eV.[51] We attempted to distinguish between the two possibilities by establishing the threshold for the second feature. To this end, we modeled the threshold region of the V^+ cross section including competition with reaction 25 and made various assumptions concerning the behavior at higher energies. Depending on these assumptions, we could obtain reasonable reproductions of the data when the threshold for the second feature is near either 2 or 3.3 eV. The lower threshold value is slightly higher than the threshold calculated for the spin-allowed formation of $V^+(a^3F)$. The upper threshold value is lower than that expected for CID. Failure to observe efficient CID would not be surprising as the low mass of D_2 renders the CID process relatively inefficient.[52] Overall, the complex shape of the V^+ cross section cannot be reliably reproduced using two models with known thermochemistry, and therefore we cannot unambiguously assign the second feature of the V^+ cross section to a specific process.

The most efficient process in the VS^+/D_2 system is the formation of VSD^+ in reaction 25.[53] The VSD^+ cross section rises from a threshold measured as 2.07 ± 0.10 eV (Table 4), peaks close to 4.5 eV, and declines at higher energies due to the dissociation of the VSD^+ product. The dissociation can occur either by formation of $VS^+ + D$, which requires 4.556 eV, or of $V^+ + SD$, which requires 4.64 ± 0.11 eV. The energy behavior of the VSD^+ cross section is consistent with either of these pathways, but there is no obvious evidence for the latter dissociation pathway in the V^+ cross section.

In the reaction of VO^+ with D_2, the formation of VD^+ was observed as a third, very inefficient channel.[50] The analogous reaction 26 represents a formal metathesis reaction, because both reactant bonds are cleaved and two new product bonds are formed. Formation of VD^+ is also observed in the reaction of VS^+ with D_2, though the VD^+ cross section is again very small ($\sigma_0 < 0.1 \times 10^{-16}$ cm^2). A threshold of 2.52 ± 0.13 eV (Table 4) is measured for process 26, in very good agreement with the calculated value of 2.55 ± 0.13 eV.

FTICR. Exothermic and slightly endothermic ($\Delta_R H < 0.2$ eV) reactions with no barriers in excess of the reactant energy can be observed in the FTICR instrument after thermalization of the precursor ions.[54] Reactions 7 and 28 represent the exothermic reversals of reactions 12 and 24, respectively, and both are observed under FTICR conditions:

$$V^+ + COS \rightarrow VS^+ + CO \qquad [-0.64 \pm 0.10 \text{ eV}]$$
$$k = 2.7 \times 10^{-10} \text{ cm}^3 \text{ molecule}^{-1} \text{ s}^{-1} \qquad (7)$$

$$V^+ + H_2S \rightarrow VS^+ + H_2 \qquad [-0.75 \pm 0.10 \text{ eV}]$$
$$k = 0.7 \times 10^{-10} \text{ cm}^3 \text{ molecule}^{-1} \text{ s}^{-1} \qquad (28)$$

The reaction rate constant of 2.7×10^{-10} cm^3 molecule^{-1} s^{-1} derived for reaction 7 from the FTICR experiment agrees with a reaction rate constant of $3.8 \pm 2 \times 10^{-10}$ cm^3 molecule^{-1}

s^{-1} that can be derived from the GIB measurements of reaction 7 within the experimental uncertainty.[13] Compared to the collision rate constants (about 1×10^{-9} cm^3 molecule^{-1} s^{-1}), both reactions proceed inefficiently, indicating there are kinetic constraints to product formation (see below).

Reactions 29 and 30 were studied in order to examine the interchange of the chalcogenide ligands:

$$VS^+ + H_2O \rightarrow VO^+ + H_2S \qquad [-0.21 \pm 0.14 \text{ eV}]$$
$$k = 1.0 \times 10^{-10} \text{ cm}^3 \text{ molecule}^{-1} \text{ s}^{-1} \quad (29)$$

$$VO^+ + H_2S \rightarrow VS^+ + H_2O \qquad [0.21 \pm 0.14 \text{ eV}]$$
$$k < 10^{-13} \text{ cm}^3 \text{ molecule}^{-1} \text{ s}^{-1} \quad (30)$$

Because reactions 29 and 30 are almost thermoneutral, there is the interesting possibility of establishing an equilibrium between VS^+ and VO^+ when both are trapped in a mixture of H_2O and H_2S. However, isolated VO^+ ions trapped in a 1:6 mixture of H_2O and H_2S for at least 10 s do not react with either H_2S or H_2O. In contrast, VS^+ ions isolated and trapped in the same mixture react readily with H_2O to form VO^+ according to reaction 29 and with H_2S to form VS_2^+ as depicted in reaction 31.

$$VS^+ + H_2S \rightarrow VS_2^+ + H_2 \qquad [<-0.11 \pm 0.01 \text{ eV}]$$
$$k = 1.0 \times 10^{-10} \text{ cm}^3 \text{ molecule}^{-1} \text{ s}^{-1} \quad (31)$$

Thus, the endothermicity of reaction 30 as well as the competing formation of VS_2^+ prevents establishment of an equilibrium between $VS^+ + H_2O$ and $VO^+ + H_2S$. We also find that VS^+ continues to react with COS to produce the VS_2^+ cation, reaction 20. The occurrence of reaction 31 under FTICR conditions leads to a lower limit for $D_0(SV^+-S)$ of 3.03 eV, which is consistent with a similar value (3.14 eV) derived from the exothermic behavior of reaction 20 in the GIB experiments.

Finally, the reactivity of V^+ ions toward CS_2 has been examined. Formation of VS^+ is indeed observed, but depends strongly on the extent of thermalization with methane. With increasing thermalization, the formation of VS^+ decreases drastically and finally vanishes at high methane pressures. This clearly indicates the involvement of electronically excited V^+ ions in reaction 2 when performed in the FTICR at low methane pressures, which helps to confirm that the first two endothermic features of the VS^+ cross section of reaction 2 measured in the GIB experiments correspond to the reaction of ground-state V^+ (^{5}D) with possible contributions from V^+(^{5}F).[20]

Sector-MS. In the HRTEL spectra of VO^+ and VS^+ (Figure 8), no peaks are observed at the high-energy sides of the main beams, thus ruling out major contributions from long-lived excited states of VX^+ (X = O, S).

In addition to the main peak at zero translational energy loss (Figure 8a), which is assigned to VO^+ in its $^3\Sigma^-$ ground state,[55] we observe two excitation peaks near 1.3 and 4.5 eV, which are due to collisional excitation of VO^+ and may be attributed to the transitions VO^+ ($^3\Sigma^-$) → VO^+ ($^3\Delta$) and VO^+ ($^3\Sigma^-$) → VO^+ ($^5\Pi/^5\Sigma^-$) (see below). In addition, dissociation of the dioxygen target, $D_0(O-O) = 5.12$ eV, contributes to the broad peak at about 5 eV. For VS^+, a similar spectrum is obtained (Figure 8b) though the signal-to-noise ratio is worse, and only one broad excitation peak near 2.0 eV is apparent.

B. Theoretical Results. To shed further light on the experiments, electronic structure calculations have been performed for VO^+ and VS^+. In addition to thermochemical information, computational methods can provide insight into the bonding situation and the electronic states of these species. The valence structure of the transition metal sulfide cation is expected to correspond to those of the analogous metal oxide cation and should lead to similar state splittings and ground state configurations. The early transition metal oxide cations form triple bonds with oxygen atoms in a similar manner as in CO except that bonding involves the d-orbitals of the metal.[56,57] The details concerning the state splittings and bonding features of VX^+ (X = O, S) obtained are summarized in Tables 5 and 6.

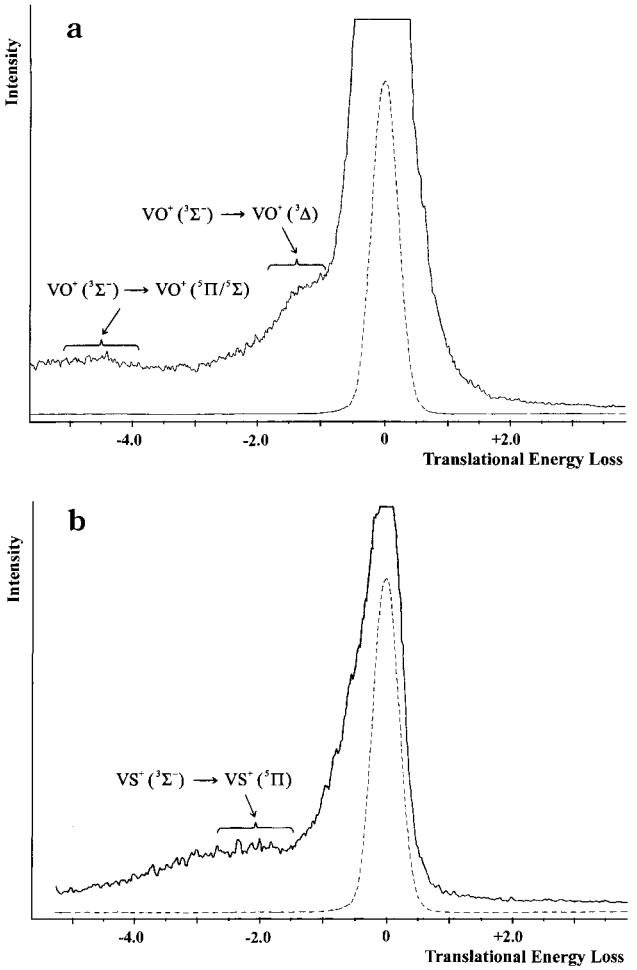

Figure 8. (a) High-resolution translational energy loss spectrum for VO^+ with O_2 as collision gas (solid line). (b) High-resolution translational energy loss spectrum for VS^+ with O_2 as collision gas (solid line). In both plots, the dotted lines represent the ion beam signals when no collision gas is present.

At all levels of theory and with all basis sets used, the $^3\Sigma^-$ state is found to be the ground state of the vanadium sulfide cation. This results from perfect pairing of V^+ (^{5}D) and S (^{3}P) with the uncoupled electrons in virtually nonbonding δ-type orbitals, giving a $(1\sigma)^2(1\pi)^4(1\delta)^2$ valence configuration. The bonding pattern is confirmed by the natural bond orbital (NBO)[58] analysis of VS^+ ($^3\Sigma^-$) which reveals that a triple bond is formed by two d electrons from V^+ and four p electrons of S. The first excited triplet ($^3\Delta$) is ca. 0.36 eV higher in energy and arises from the formal excitation of one electron from a nonbonding δ-type orbital to the lowest antibonding σ-type orbital, i.e., a $(1\sigma)^2(1\pi)^4(1\delta)^1(2\sigma)^1$ configuration. The adiabatic excitation energy to the lowest-lying quintet state ($^5\Pi$) is 1.37 eV, while vertical excitation requires 1.87 eV. The large difference in adiabatic and vertical excitations can be attributed to the promotion of one electron from a doubly occupied

TABLE 5: State Splittings (in eV) for the First Excited Triplet and Quintet States of VX^+ (X = O, S) at the ADF/BP and MR-ACPF Level of Theory Relative to the $^3\Sigma^-$ Ground State[a]

	ADF/NP		MR-ACPF			
symmetry	r (V^+−X) [Å]		BS I	BS II	BS III	BS IV
X = S						
$^3\Sigma^-$	2.027	0.00	0.00	0.00	0.00	0.00
$^3\Delta$	2.028	0.59[b]	0.23	0.34	0.36	0.36
$^5\Pi$ (adiabatic)	2.210	1.59[c]	1.22	1.33	1.34	1.37
$^5\Pi$ (vertical)	2.027	1.90	1.74	1.85	1.84	1.87
X = O						
$^3\Sigma^-$	1.554	0.00	0.00	0.00	0.00	
$^3\Delta$	1.573	1.46[d]	1.14	1.34	1.36	
$^5\Sigma^-$ (adiabatic)	1.822	3.76	2.69	2.73	2.81	
$^5\Sigma^-$ (vertical)	1.554	4.85	4.37	4.35	4.39	
$^5\Pi$ (adiabatic)	1.806	3.69	3.02	3.13	3.18	
$^5\Pi$ (vertical)	1.554	5.16	4.49	4.65	4.66	

[a] Total MR-ACPF energies in Hartree for VS^+ ($^3\Sigma^-$): −468.51673 (BS I), −1340.41482 (BS II), −1340.43269 (BS III), and −1340.43722 (BS IV); total MR-ACPF energies for VO^+ ($^3\Sigma^-$) −145.90487 (BS I), −1070.81227 (BS II), and −1017.82994 (BS III). [b] Adiabatic excitation energies for the next higher triplet states of VS^+ at this level of theory: $^3\Pi/^3\Phi$ =1.22 eV, $^3\Sigma/^3\Delta$ = 2.96 eV. [c] Adiabatic excitation energy to the next higher quintet state of VS^+ at this level of theory: $^5\Sigma$ =1.94 eV. [d] Adiabatic excitation energies for the next higher triplet states of VO^+ at this level of theory: $^3\Pi/^3\Phi$ =1.74 eV, $^3\Sigma/^3\Delta$ = 3.81 eV.

TABLE 6: Bond Dissociation Energies (D_0) at the MCSCF and MR-ACPF Level of Theory

	D_0 (V^+−S)[a] [eV]		D_0 (S−S)[b] [eV]		D_0 (V^+−O)[c] [eV]	
level of theory	MCSCF	MR-ACPF	MCSCF	MR-ACPF	MCSCF	MR-ACPF
BS I	2.89	3.35	3.00	3.76	5.36	5.58
BS II	2.94	3.42	3.20	3.98	5.35	5.51
BS III	3.00	3.60	3.36	4.33	5.43	5.71
BS IV	3.01	3.66	3.38	4.41		
exptl	3.78 (0.10)[d]		4.364 (0.005)[e]		5.99 (0.10)[f]	

[a] ZPVE(V^+−S) = 0.03 eV. [b] ZPVE(S−S) = 0.04 eV. [c] ZPVE(V^+−O) = 0.07 eV. [d] This work. [e] Table 3. [f] Ref 59.

bonding π-orbital to the lowest antibonding σ-orbital, i.e., a $(1\sigma)^2(1\pi)^3(1\delta)^2(2\sigma)^1$ configuration. The occupation of the antibonding σ-orbital causes an elongation of the VS^+ bond in the quintet state by 0.31 Å. Table 6 summarizes the bond dissociation energies of VS^+ and of the S_2 molecule calculated with different basis sets for the description of vanadium and sulfur (see Experimental Section). $D_e(V^+-S)$ is calculated to be 3.69 eV at the MR-ACPF level of theory using BS IV, which leads to $D_0(V^+-S)$ = 3.66 eV after ZPVE correction. This value agrees nicely with the experimentally determined $D_0(V^+-S)$ = 3.78 ± 0.10 eV.

In close analogy to VS^+, a $^3\Sigma^-$ ground state for VO^+ was found with a low-lying triplet excited state ($^3\Delta$) at 1.36 eV. Experimental values for the excitation energy are 1.04 ± 0.09[44] and 1.17 ± 0.02 eV.[55a] The lowest quintet states correspond to VO^+ ($^5\Sigma^-$) and VO^+ ($^5\Pi$) which are 2.81 and 3.18 eV (Table 5) above the VO^+ ($^3\Sigma^-$) ground state, respectively. An experimental value for the adiabatic excitation energy to the quintet states of VO^+ is 3.11 ± 0.31 eV,[44] in good agreement with the calculated values. The order is reversed for VS^+ ($^5\Sigma^-$) and VS^+ ($^5\Pi$). The large difference between the adiabatic and vertical VO^+ ($^3\Sigma^-$) → VO^+ ($^5\Pi/^5\Sigma^-$) excitation (Table 5) can be explained invoking the same effect outlined for VS^+. The calculated bond dissociation energy of VO^+ after ZPVE correction is 5.71 eV at the ACPF level of theory with BS III (Table 6) which compares reasonably well with the experimental value of $D_0(V^+-O)$ = 5.99 ± 0.10.[10,59]

Discussion

The discussion is organized in the following way. First, we consider the formation of VS^+ in reaction 2. Next, the shifts in the apparent thresholds for formation of V^+ upon CID of VS^+ are related to the nature of the collision gas used. As V^+ can also be formed in ion−molecule processes of VS^+, e.g., reactions 12, 21, and 24, their thresholds are used as independent measures of the V^+−S bond energy. Then we analyze production of VO^+, which is formed in all reactions of VS^+ with neutral molecules containing oxygen. Finally, the thresholds of the cross sections for VCS^+ and VSD^+ are investigated, providing the first experimental values for $D_0(V^+-CS)$ and $D_0(V^+-SD)$. Following the discussion of these various product channels, the reliable individual determinations of the VS^+ bond energy are pooled to generate our best experimental estimate of $D_0(V^+-S)$, which is then compared to the theoretically determined value. Finally, the shapes of the VS^+ cross sections for reactions 2 and 7 are compared qualitatively and interpreted in terms of the production of an electronically excited state. Quantitative estimates of the excitation energy ($^3\Sigma^- \rightarrow {}^5\Sigma^-$) are then compared with the value derived from the calculations.

VS^+. The VS^+ cross section shown in Figure 1 has three endothermic features. As mentioned above, the first two features must correspond to reaction 2. A careful and extensive experimental study of the VS^+ cross section and its features has been performed in which the electronic state distribution of the V^+ reactant was varied using different ion sources, such as electron ionization (EI), surface ionization (SI), and dc discharge/flow tube sources.[20] Several cross section models were employed in the threshold analysis of the data, and a threshold of 0.78 ± 0.08 eV for the first low-energy feature of the VS^+ cross section is derived.[20] Using this threshold and the thermochemical data given in Tables 2 and 3, we arrive at $D_0(V^+-S)$ = 3.72 ± 0.09 eV.

V^+. The formation of V^+ from VS^+ is observed with all neutral targets used in the GIB experiments. The processes leading to V^+ can be divided into two categories, i.e., bond cleavages in collision-induced dissociation and chemical transformations involving the formation of other bonds. Careful investigations of systematic effects on the threshold analysis for low-energy CID processes have been reported previously.[21a,60] The following conclusions have been drawn. (i) Parent ions created with an excess of internal energy give rise to a shift of the CID threshold to lower energies,[61] therefore appropriate cooling is required. This should not be a problem in the present work because the ions have been thermalized before reaction. (ii) As the number of degrees of freedom in the dissociating ions increases, the lifetime of the collisionally activated complex increases and can become the same order of magnitude as the time the ions need to pass through the instrument.[21a] Lifetime effects in dissociation should not be a factor in the present study because VS^+ is a diatomic molecule. (iii) The nature of the collision gas used can also influence the CID cross section. As the number of degrees of freedom increases, the neutral molecule can carry away more energy from the collision complex in internal modes, thereby leading to less efficient kinetic-to-internal energy transfer to the ion during the collision. This can cause the cross section to rise more slowly which leads to elevated thresholds obtained in the analysis. (iv) The mass of the collision gas used has a distinct effect on the CID process. The lighter the neutral reactant, the more energy is necessary

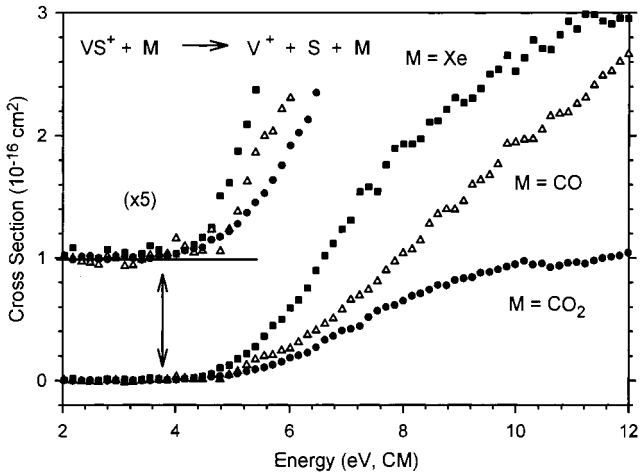

Figure 9. CID cross sections for formation of V^+ from VS^+ with the targets, Xe (■), CO (△), and CO_2 (●), as a function of center-of-mass energy (lower axis). The cross section shown for CID of VS^+ with CO is the cross section obtained after subtraction of the small low-energy feature associated with process 12. The inset shows the threshold region of the V^+ cross section for all three targets on an expanded vertical scale and offset from zero by 1×10^{-16} cm^2. The arrow marks the dissociation energy of VS^+ at 3.78 eV.

to provide a certain center of mass energy, giving the reactants less time to interact, which may decrease the efficiency of kinetic-to-internal energy transfer during the collision. Again, this can cause the corresponding cross sections to rise more slowly and renders the determination of the threshold more difficult. (v) The strength of the interaction between the ion and the collision gas influences the lifetime of the collision complex. More strongly bound species will have more time to interact, leading to more efficient energy transfer at hyperthermal energies. Factors iii−v are relevant here.

The CID cross sections determined in this study are collected in Figure 9. Note, that the cross section shown for M = CO is the cross section shown in Figure 4 *after* subtracting a model of the small low-energy feature attributed to process 12. These cross sections illustrate the effects noted above. Clearly, the dissociation probability is reduced for collisions with CO and CO_2 compared with Xe. This is largely the mass effect discussed above in factor iv. We also find that although CO is lighter than CO_2, it seems to be a more efficient CID gas. This observation is most easily rationalized by the nature of the gas (factor iii), and the strength of the interaction (factor v). The latter factor is illustrated by the V^+−CO bond energy, 1.17 eV,[62] which is larger than that for V^+−CO_2, 0.75 eV.[44] Because these cross sections rise so slowly from threshold, analysis of the kinetic energy dependence using eq 1 tends to give thresholds that are higher than the V^+−S bond dissociation energy derived from ion−molecule reactions. Thus, these CID thresholds can only be regarded as upper limits for $D_0(V^+-S)$.[21a] Similar behavior has also been observed in previous studies concerning CID of VO^+ and other metal oxide cations.[63,64]

The situation is different for the thresholds of the non-CID processes, reactions 12, 21, and 24. Using the thresholds given in Table 4 and the thermochemical data given in Tables 2 and 3, one arrives at $D_0(V^+-S) = 4.02 \pm 0.40$ eV, 3.64 ± 0.18 eV, and 3.85 ± 0.08 eV, respectively. The large uncertainty for reaction 12 can be attributed to the small magnitude (0.16×10^{-16} cm^2) of the cross section and the complication of the higher energy and more efficient CID process 14. It is also possible that the threshold of reaction 12 is slightly elevated because excited-state low-spin V^+ ions are formed preferentially, a consequence of reaction 12 being a spin-forbidden process when ground-state V^+ (^{5}D) ions are produced. To ensure that there are no significant activation barriers in excess of the endothermicities of reactions 12 and 24, the reverse reactions 7 and 28 were measured with the FTICR. Both reactions were found to occur, though inefficiently (see above). These low efficiencies can be rationalized by the fact that both reactions are spin-forbidden.

VO^+. The formation of VO^+ is observed in three reactions between VS^+ and oxygen-bearing reactants, CO, CO_2, and COS, and also in the reaction of V^+ with COS. From Figures 2, 4, and 6, it is obvious that the O-transfer and the sulfur−oxygen exchange processes are inefficient for CO and COS (σ_{max} ca. 0.5×10^{-16} cm^2), while the VO^+ formation is three times more efficient with CO_2 (Figure 5). Because the cross sections rise slowly and are small, the determinations of the thresholds of reactions 13 and 23 have large uncertainties (Table 4) and lead to $D_0(V^+-S) = 5.21 \pm 0.49$ eV and 3.67 ± 0.49 eV, respectively. While the latter value is consistent with the values reported above, the value obtained from reaction 13 is much larger and points to the operation of significant kinetic effects that may simply be the result of a metathesis reaction involving the simultaneous cleavage and formation of several multiple bonds. The low efficiencies (σ_{max} ca. 0.5×10^{-16} cm^2) of reactions 13 and 23 can be rationalized by the high C−O bond energies in CO (11.109 ± 0.005 eV) and COS (6.88 ± 0.04 eV), the restricted transition structures associated with the formal O/S metathesis, and the presence of an efficient competing channel, i.e., the formation of VS_2^+ in process 20 in the reaction of COS with VS^+. The influence of the C−O bond energies and the occurrence of side reactions become evident from the comparison of the cross section for the formation of VO^+ in reactions 13 and 23 with that in reaction 18. The OC−O bond energy of 5.453 ± 0.002 eV is significantly lower than D_0(SC−O) and D_0(C−O). Except for collision-induced dissociation and the very inefficient formation of VOS^+, no other product channels are observed in the CO_2 system. Further, the observation of VOS^+ formation in the reaction of VS^+ with CO_2 (but not with CO and COS) also points to much better O-transfer probability from the CO_2 target. Unfortunately, VO^+ is formed via two different pathways in the reaction of VS^+ with CO_2, processes 16 and 18, which complicates the cross-section analysis enough that it is not possible to derive a meaningful threshold for either process.

In conclusion, CO_2 is a much better sulfur−oxygen exchange reagent for the early transition metal sulfide cations than CO and COS. Despite the strong metal−oxygen bond of the early transition metal oxide cations, $D_0(M^+-O) > 5.98$ eV,[10] which is a driving force for sulfur−oxygen interchange, the high C−O bond energies in these neutrals lower the overall efficiencies of the S/O exchange reactions, leading to large uncertainties in the threshold determinations. The occurrence of a more efficient sulfur-transfer reaction in the case of COS makes the situation even worse.

VD^+. The thermochemistry of VD^+ (Table 2) is well established[65] and can be used for one additional independent determination of the VS^+ bond energy. Even though the VD^+ species formed in reaction 26 has a small cross section, analysis yields a reasonably precise threshold of 2.52 ± 0.13 eV (Table 4). This corresponds to a bond dissociation energy of $D_0(V^+-S) = 3.75 \pm 0.15$ eV.

VCS^+. In the reaction of V^+ with CS_2, the formation of VCS^+ according to reaction 3 is observed with a threshold of 2.80 ± 0.07 eV.[20] The threshold can be converted to $D_0(V^+-$

CS) = 1.70 ± 0.08 eV using the thermochemical data given in Tables 2 and 3. The VCS^+ ion is most likely a thiocarbonyl complex of the vanadium cation. The CS ligand can be formed by insertion of the metal ion into a C−S bond of CS_2 followed by loss of the sulfur atom attached to the metal center. The VCS^+ connectivity is further supported by the formation of VCO^+ rather than OVC^+ in the analogous reaction of V^+ with CO_2.[44]

Comparison of the D_0 values for VCO^+ and VCS^+ (Table 2) shows that the CS ligand is bound more strongly by 0.53 ± 0.09 eV. CS should be a better σ-donor than CO simply because it has a higher polarizability. The CS ligand is also a better π-acceptor than CO, as supported by theoretical studies[66] as well as crystallographic data of mixed transition metal complexes with CO and CS ligands.[67] In some of these complexes, the M−CS bonds are about 0.05 Å shorter than the corresponding M−CO bonds. Further, MO-SDCI calculations predict the bond length of neutral V−CO to be 0.04 Å longer than the V−CS bond.[68] These findings imply that there is a stronger synergetic interaction of the metal atom with the thiocarbonyl ligand than with carbon monoxide. Interestingly, the thiocarbonyl ligand can still react as a nucleophile while the CO ligand in VCO^+ cannot.[67]

VSD^+. The VSD^+ cation formed in reaction 25 can conceivably have two structures. Either it contains an intact SD ligand (VSD^+), or the deuterium atom is bound to the metal (DVS^+). One can think of the binding situation in the latter by noting that there are two singly occupied nonbonding δ-orbitals in VS^+ that can interact with the deuterium atom. A covalent V−D bond would lead to a bent structure, because the δ-orbitals are orthogonal to the π- and σ-orbitals forming the V−S triple bond. Thus, a doublet ground state is expected for the DVS^+ isomer. The binding situation is somewhat different in VSD^+. Here, it is no longer possible for sulfur to form a triple bond with vanadium, because one of the valence electrons of sulfur is already used for the S−D bond. Thus, there remain only one unpaired electron and a lone pair of electrons at the sulfur to form a bond with V^+. Following this bonding scheme, VSD^+ should have a high-spin quartet ground state.

Calculations using the B3LYP/6-311+G* level of theory predict VSH^+ ($^4A''$) to be more stable than HVS^+ ($^2A'$) by 1.33 eV. NBO analyses are fully in line with the bonding descriptions outlined above.[69] Further, VSH^+ exhibits a bent structure with a VSH angle of 99° which is in close analogy to the HSH angle of 92.1° in hydrogen sulfide and points to a similar hybridization at the sulfur center in both species. In conclusion, the VSD^+ ion formed in reaction 25 has an intact DS ligand. Using the thermochemistry given in Tables 2 and 3, $D_0(V^+-SD)$ is derived as 2.57 ± 0.15 eV. The bond strength in the V^+-SD is only about 60% of that in the oxygen analogue V^+-OD, (4.50 ± 0.15 eV).[43] This result is consistent with the results of MCSCF(CI) calculations performed on the comparable $ScOH^+/ScSH^+$ systems where a factor of 53% has been found.[70] Interestingly, the authors find a linear structure for $ScSH^+$ in contrast to the bent structure found in our study for VSH^+. As discussed in detail elsewhere,[8c] the V^+-OH bond is much stronger than $D_0(V^+-CH_3)$ = 2.00 ± 0.07 eV because two lone pairs of electrons on the oxygen can donate into empty or singly occupied 3dπ-orbitals on the metal. Assuming this bonding pattern, VOH^+ is expected to be linear.[8c] Indeed, preliminary calculations of VOH^+ ($^4A''$) at the B3LYP/6-311+G* level of theory predict an almost linear geometry (V−O−H angle 173°), which is separated from the linear structure by only 1×10^{-4} eV.[68] Because this energy difference is lower than the zero-point energy, VOH^+ can be considered as a quasi-linear molecule.[71] Linear geometries are also reported for $ScOH^+$ and $TiOH^+$ at the B3LYP level of theory.[72] The linear structure of VOH^+ is in marked contrast to the bent structure found for VSH^+. Hence, π-dative interactions appear to be reduced significantly in VSH^+ as compared to VOH^+.

$D_0(V^+-S)$. From reactions 2, 12, 21, 23, 24, and 26, we obtain $D_0(V^+-S)$ = 3.72 ± 0.09, 4.02 ± 0.40, 3.64 ± 0.18, 3.67 ± 0.49, 3.85 ± 0.08, and 3.75 ± 0.15 eV, respectively. The weighted average of these values[73] is calculated to be 3.78 ± 0.10 eV where the uncertainty is two standard deviations of the mean.

Comparison of the experimental (3.78 ± 0.10 eV) and the calculated bond dissociation energy (3.66 eV) shows excellent agreement between experiment and theory. A reduction of the calculated bond dissociation energy by ca. 0.02 eV arises from estimation of the different spin−orbit couplings (SOC) in the V^+ and VS^+ ions.[74] A minor underestimation of the calculated bond dissociation energy can be assigned to limitations of the basis sets as well as a still insufficient description of the bonding at the MR-ACPF level of theory. To evaluate the quality of the basis sets used for sulfur, the bond dissociation energy of the S_2 molecule was calculated (Table 6). The following conclusions can be drawn when comparing the experimental and theoretical values for D_0(S−S). (i) The MCSCF level of theory is insufficient for an exact description of the bonding in S_2 because it does not include dynamic correlation. (ii) The MR-ACPF calculations include dynamic correlation and therefore are capable of describing the bonding situation more correctly. (iii) Finally, the sulfur basis is almost saturated in BS IV after addition of one *g* function. The minor overestimation of D_0(S−S) can be attributed to basis-set superposition error (BSSE),[75] which will somewhat lower the calculated bond energy. These minor effects are not considered any further in this study. Although the vanadium basis sets are quite large, they are still far from being saturated. Further enlargement of the vanadium basis would, however, cause a substantial increase in computation time. In view of the expected relatively small improvement of the accuracies, performing calculations at such a level seemed unreasonable to us.

One aspect of our calculations deserves comment. A common and natural choice of active space for multireference calculations includes all valence electrons and orbitals. In the present case, this would also comprise the 3s-orbital of sulfur, which was *not* included in the active space of our calculations. When the 3s-orbital of sulfur is included, it mixes with the inner-shell $3p_z$-orbital of vanadium, leading to a strongly reduced value for the calculated $D_0(V^+-S)$ (3.31 eV with MR-ACPF/BS IV). This is because of an unbalanced treatment of the VS^+ molecule and the isolated atoms. In the latter, correlation of the sulfur 3s-orbital is included, and leads to a significant decrease in the total energy. In the molecule, the σ-orbital which is correlated has partly sulfur 3s and partly vanadium $3p_z$ character. Because the correlation energy for the latter is much smaller, the decrease in total energy for the molecule is also much smaller than it should be, leading to the observed low value for the calculated D_0. We suggest that a similar $3s/3p_z$ mixing may be the reason for the sizable deviation of the calculated bond energy of 4.08 eV for the neutral VS as reported by Bauschlicher and Maitre[76] from the experimental value (4.62 eV).[77] These authors noted the occurrence of such a mixing for the neutral scandium and titanium sulfides, but unfortunately did not address this issue in their calculation of D_0(V−S). Inclusion of the 3s- and 3p-orbitals of vanadium in the active space may improve the

accuracy of the theoretical prediction, but this would have exceeded our computational resources.

Excited States of VS^+. The second low-energy feature of the VS^+ cross section of reaction 2 (Figure 1) has been determined elsewhere[20] to have a threshold of 2.23 ± 0.14 eV, which is 1.45 ± 0.16 eV above the lowest threshold. A similar bimodal behavior is observed in the VS^+ cross section obtained for the V^+/COS system, with the difference that the first feature is exothermic (Figure 2). The rationale for this observation can be found in the different C−S bond strengths in CS_2 (4.50 ± 0.04 eV) and COS (3.140 ± 0.005 eV). Thus, sulfur transfer from COS should be 1.36 eV less endothermic than from CS_2, which causes reaction 7 to become exothermic. An estimate of 1.44 ± 0.14 eV for the energy difference of the two features in the V^+/COS system can be obtained by adding the reaction enthalpy $\Delta_R H = -0.64 \pm 0.10$ eV of reaction 7 and the threshold for the endothermic feature (0.8 ± 0.1 eV). Thus, the splittings obtained from the two VS^+ cross sections, 1.45 ± 0.16 eV[20] and 1.44 ± 0.14 eV, agree nicely and have an average value of 1.44 ± 0.13 eV.

The experiments with CS_2 and COS were performed under similar conditions, and one can assume that the distributions of electronic states in the V^+ beam are equivalent. Further, COS and CS_2 are isoelectronic, both having $^1\Sigma^+$ electronic ground states.[22] Thermodynamic considerations also exclude the formation of VS^+ via routes different than reactions 2 or 7. Thus, the only explanation for the observation of the second features in both VS^+ cross sections is the formation of either VS^+ or the neutral products (CO/CS) in states other than their ground states. Both CS and CO have $^1\Sigma^+$ ground states,[22] and excitations into the $^1\Pi$ first excited states require 4.82 and 8.07 eV,[22] respectively, much too high to explain the experimental observations. Thus, the only reasonable explanation for the observation of two features in both VS^+ cross sections is the formation of VS^+ in two different electronic states.

The experimental state splitting of 1.44 ± 0.13 eV correlates well with the calculated splitting for the lowest quintet state ($^5\Pi$), 1.37 eV above the ground state. Thus, we attribute the second feature in the VS^+ cross sections of reactions 2 and 7 to the formation of VS^+ ($^5\Pi$). Consideration of the spin multiplicities of the reactants and products involved in reactions 2 and 7 reveals that the process leading from ground-state reactants to the formation of ground-state VS^+ ($^3\Sigma^-$) is spin-forbidden, while formation of excited-state VS^+ ($^5\Pi$) is spin-allowed. The formation of VS^+ ($^3\Sigma^-$) in reactions 2 and 7 at the respective thermodynamic thresholds[20] is another manifestation of two-state reactivity (TSR),[57,78,79] in which two states of different multiplicities determine the minimum-energy pathway of a reaction.

The calculated state splittings for VO^+ and VS^+ are also capable of explaining the peaks observed in the HRTELS study. These experiments monitor vertical excitations of the precursor ions to higher states, and a rough estimate for the state splitting can be derived from the peak-to-peak distances. Thus, the shoulder near 1.3 eV in the energy loss spectrum of VO^+ (Figure 8a) can be assigned to the $^3\Sigma^- \rightarrow {}^3\Delta$ transition, which has a calculated splitting of 1.36 eV. The broad peak near 4.5 eV can be attributed to the vertical $^3\Sigma^- \rightarrow {}^5\Sigma/{}^5\Pi$ transitions, which have calculated splittings of 4.39 and 4.66 eV (Table 5). The latter peak is broadened by several factors in addition to beam scattering. First, the HRTELS experiment should probe not only the $\nu = 0 \rightarrow \nu' = 0$ transition but all allowed transitions. Second, the energy spacing between the VO^+ ($^5\Sigma$) and VO^+ ($^5\Pi$) states is small, and both are likely to be populated. Finally, the substantial bond elongation from the triplet to the quintet states favors transitions other than the $0 \rightarrow 0$ transition. In the case of VS^+, the calculations predict 0.36 eV for the $^3\Sigma^-/{}^3\Delta$ splitting. This difference is too small to be resolved in the HRTELS experiment (Figure 8b) due to the limited energy resolution (0.5 eV), collisional broadening, and the vibrational progression leading to a tailing at the low-energy side of the incident beam. However, a distinct peak is observed at about 2.0 eV. We attribute this to the vertical $^3\Sigma^- \rightarrow {}^5\Pi$ transition in VS^+ which has a calculated splitting of 1.87 eV (Table 5). Again, this peak is broadened by a vibrational progression. Notwithstanding the limited resolution of the experiments, the calculated energies of the triplet and quintet states of VX^+ (X = O, S) are in good qualitative agreement with the results obtained with GIB and HRTELS.

Conclusions

The bond dissociation energy of VS^+, $D_0(V^+-S) = 3.78 \pm 0.10$ eV, has been derived by studying six different chemical reactions. The good agreement between this value and that derived in the V^+ (^5D) + CS_2 reaction shows that the formation of VS^+ in its triplet ground state from the reaction of $V^+ + CS_2$ has no activation barrier in excess of the reaction endothermicity. Considering that the formation of ground-state VS^+ involves a spin-forbidden process, the occurrence of VS^+ at the thermochemical threshold in the reactions of V^+ with CS_2 and COS is a case of two-state reactivity. At elevated energies, the spin-allowed formation of VS^+ ($^5\Pi$) competes efficiently with the lower-energy, spin-forbidden process. Further, the calculated adiabatic and vertical state splittings agree favorably with those derived from GIB experiments and HRTELS data. Indeed, a combination of various experimental and theoretical approaches as performed in this study opens up promising perspectives of transition metal chemistry in the gas phase with explicit consideration of excited states. Nevertheless, the ability of the experimental tools used in this study to accurately probe electronic state separations is limited. Clearly, other experimental approaches are desirable in order to evaluate quantitatively the performance of the theoretical tools. Finally, the present study suggests that sulfur transfer reactions between CS_2 and M^+ are a suitable method for determining the thermochemical properties of transition metal sulfides and are interesting systems for examining spin changes.

Acknowledgment. This research was supported by the Deutsche Forschungsgemeinschaft, the Volkswagen-Stiftung, the Fonds der Chemischen Industrie (scholarship for I.K.), and the National Science Foundation (P.B.A.), CHE-9530412. D.S. thanks the Auswärtiges Amt for a travel support. C.R. thanks the University of Utah for a research grant. Furthermore, we appreciate helpful discussions with Drs. J. N. Harvey and Dipl.-Chem. G. Hornung and are grateful to the reviewers for helpful comments.

References and Notes

(1) Takakuwa, S. In *Organic Sulfur Chemistry, Biochemical Aspects*; Oae, S., Okyama, T., Eds.; CRC Press: Boca Raton, FL, 1992; p 1. (b) Williamson, M. A.; Rimstidt, J. D. *Geochim. Cosmochim. Acta* **1992**, *56*, 3867. (c) Brandt, C.; van Eldik, R. *Chem. Rev.* **1995**, *95*, 119.

(2) (a) *Bioanorganische Chemie*; Kaim, W., Schwederski, B., Eds.; Teubner: Stuttgart, 1991. (b) Lippard, S. J.; Berg, J. M. *Principles of Bioinorganic Chemistry*; University Science Books: Mill Valley, CO., 1994.

(3) (a) Rehder, D. *Angew. Chem., Int. Ed.* **1991**, *30*, 148. (b) Butler, A.; Carrano, C. J. *Coord. Chem. Rev.* **1991**, *109*, 61.

(4) *Transition Metal Sulfur Chemistry*; Stiefel, E. I., Matsumoto, K., Eds.; ACS Symposium Series 653, American Chemical Society: Washington, DC, 1996.

(5) (a) Rosenberger, C.; Schrock, R. R.; Davis, W. M. *Inorg. Chem.* **1997**, *36*, 123. (b) Deng, Y.; Liu, Q.; Yang, Y.; Wang, Y.; Cai, Y.; Wu, D.; Chen, C.; Liao, D.; Kang, B.; Lu, J. *Inorg. Chem.* **1997**, *36*, 214. (c) See also: Do, Y.; Simhon, E. D.; Holm, R. H. *Inorg. Chem.* **1985**, *24*, 4635.

(6) (a) Bolinger, C. M.; Weatherill, T. D.; Rauchfuss, T. B.; Rheingold, A. L.; Day, C, S.; Wilson, S. R. *Inorg. Chem.* **1986**, *25*, 634. (b) Yang, Y.; Liu, Q.; Kang, B.; Lu, J. *Sci. China* **1995**, *B38*, 264. (c) Liu, Q.; Yang, Y.; Huang, L.; Wu, D.; Kang, B.; Chen, C.; Deng, Y.; Lu, J. *Inorg. Chem.* **1995**, *34*, 1884.

(7) Bhadure, M.; Mitchell, P. C. H. *J. Catal.* **1982**, *77*, 132.

(8) (a) Eller, K.; Schwarz, H. *Chem. Rev.* **1991**, *91*, 1121. (b) Freiser, B. S. *Acc. Chem. Res.* **1994**, *27*, 353. (c) Armentrout, P. B.; Kickel, B. L. In *Organometallic Ion Chemistry*; Freiser, B. S., Ed.; Kluwer Academic Publishers: Dordrecht, 1996; p 1.

(9) Schröder, D.; Schwarz, H. *Angew. Chem., Int. Ed.* **1995**, *34*, 1973, and references therein.

(10) Fisher, E. R.; Elkind, J. L.; Clemmer, D. E.; Georgiadis, R.; Loh, S. K.; Aristov, N.; Sunderlin, L. S.; Armentrout, P. B. *J. Chem. Phys.* **1990**, *93*, 2676.

(11) (a) Müller, A.; Diemann, E.; Jostes, R.; Bögge, H. *Angew. Chem.* **1981**, *93*, 957. (b) Carlin, T. J.; Wise, M. B.; Freiser, B. S. *Inorg. Chem.* **1981**, *20*, 2745. (c) Jackson, T. C.; Carlin, T. J.; Freiser, B. S. *Int. J. Mass Spectrom. Ion Processes* **1986**, *72*, 169. (d) McMahon, T. J.; Jackson, T. C.; Freiser, B. S. *J. Am. Chem. Soc.* **1989**, *111*, 421. (e) Dance, I. G.; Fisher, K. J.; Willett, G. D. *Angew. Chem., Int. Ed.* **1995**, *34*, 201. (f) Dance, I. G.; Fisher, K. J.; Willett, G. D. *Inorg. Chem.* **1996**, *35*, 4177. (g) Harvey, J. N.; Heinemann, C.; Fiedler, A.; Schröder, D.; Schwarz, H. *Chem. Eur. J.* **1996**, *2*, 1230. (h) Kretzschmar, I.; Fiedler, A.; Harvey, J. N.; Schröder, D.; Schwarz, H. *J. Phys. Chem. A* **1997**, *101*, 6252. (i) Kretzschmar, I.; Schröder, D.; Schwarz, H. *Int. J. Mass Spectrom. Ion Processes* **1997**, *167/168*, 103. (j) Fisher, K.; Dance, I.; Willett, G. *J. C. S. Dalton Trans.* **1998**, 975.

(12) For metal-sulfide clusters, see: (a) Ramli, E.; Rauchfuss, T. B.; Stern, C. L. *J. Am. Chem. Soc.* **1990**, *112*, 4043. (b) Nakat, J. H. E.; Dance, I. G.; Fisher, K. J.; Rice, D.; Willett, G. D. *J. Am. Chem. Soc.* **1991**, *113*, 5141. (c) Dehen, S.; Schäfer, A.; Ahlrichs, R.; Fenske, D. *Chem. Eur. J.* **1996**, *2*, 429. (d) Fisher, K.; Dance, I.; Willett, G.; Yi, M. *J. Chem. Soc., Dalton Trans.* **1996**, 709. (e) Nakajima, A.; Hayase, T.; Hayakawa, F.; Kaya, K. *Chem. Phys. Lett.* **1997**, *280*, 381. (f) Harvey, J. N.; Schröder, D.; Schwarz, H. *Inorg. Chim. Acta* **1998**, *273*, 111.

(13) Ervin, K. M.; Armentrout, P. B. *J. Chem. Phys.* **1985**, *83*, 166.

(14) Schultz, R. H.; Armentrout, P. B. *Int. J. Mass Spectrom. Ion Processes* **1991**, *107*, 29.

(15) (a) Eller, K.; Schwarz, H. *Int. J. Mass Spectrom. Ion Processes* **1989**, *93*, 243. (b) Eller, K.; Zummack, W.; Schwarz, H. *J. Am. Chem. Soc.* **1990**, *112*, 621.

(16) (a) Srinivas, R.; Sülzle, D.; Weiske, T.; Schwarz, H. *Int. J. Mass Spectrom. Ion Processes* **1991**, *107*, 368. (b) Srinivas, R.; Sülzle, D.; Koch, W.; DePuy, C. H.; Schwarz, H. *J. Am. Chem. Soc.* **1991**, *113*, 5970.

(17) (a) Kemper, P. R.; Bowers, M. T. *J. Phys. Chem.* **1991**, *95*, 5134. (b) Haynes, C. L.; Armentrout, P. B. *Organometallics* **1994**, *13*, 3480.

(18) (a) Aristov, N.; Armentrout, P. B. *J. Phys. Chem.* **1987**, *91*, 6178. (b) Clemmer, D. E.; Sunderlin, L. S.; Armentrout, P. B. *J. Phys. Chem.* **1990**, *94*, 208.

(19) Moore, C. E. *Atomic Energy Levels*, National Standard Reference Data Series, National Bureau of Standards, NSRDS-NBS 35, Washington, D.C., 1971.

(20) Rue, C.; Armentrout, P. B.; Kretzschmar, I.; Harvey, J. N.; Schröder, D.; Schwarz, H. In preparation.

(21) (a) Schultz, R. H.; Crellin, K. C.; Armentrout, P. B. *J. Am. Chem. Soc.* **1991**, *113*, 8590. (b) Armentrout, P. B. In *Advances in Gas-Phase Ion Chemistry*; Adams, N. G., Babock, L. M., Eds.; JAI Press: Greenwich, 1992; Vol. 1, pp 83−119.

(22) Herzberg, G. In *Molecular Spectra and Molecular Structure*, reprint edition; Krieger: Malabar, 1989; Vol. I.; and 1991; Vol. III.

(23) Chesnavich, W. J.; Bowers, M. T. *J. Phys. Chem.* **1979**, *83*, 900.

(24) See, for example: Sunderlin, L. S.; Armentrout, P. B. *Int. J. Mass Spectrom. Ion Processes* **1989**, *94*, 149.

(25) (a) Khan, F. A.; Clemmer, D. C.; Schultz, R. H.; Armentrout, P. B. *J. Phys. Chem.* **1993**, *97*, 7978. (b) Dalleska, N. F.; Honma, K.; Sunderlin, L. S.; Armentrout, P. B. *J. Am. Chem. Soc.* **1994**, *116*, 3519. (c) Dalleska, N. F.; Honma, K.; Armentrout, P. B. *J. Am. Chem. Soc.* **1993**, *115*, 12125.

(26) Rodgers, M. T.; Armentrout, P. B. *J. Phys. Chem. A* **1997**, *101*, 2614.

(27) Front-end resolution enhancement with tailored sweeps: Forbes, R. A.; Laukien, F. H.; Wronka, J. *Int. J. Mass Spectrom. Ion Processes* **1988**, *83*, 23.

(28) (a) *Collision Spectroscopy*; Cooks, R. G., Ed.; Plenum Press: New York, 1978. (b) Illies, A. J.; Bowers, M. T. *Chem. Phys.* **1982**, *65*, 281. (c) Rabrenovic, M.; Ast, T.; Beynon, J. H. *Int. J. Mass Spectrom. Ion Processes* **1985**, *61*, 31. (d) Jonathan, P.; Hermann, Z.; Hamdan, M.; Breton, A. G. *Int. J. Mass Spectrom. Ion Processes* **1988**, *84*, 203. (e) Schulze, C.; Schwarz, H. *Chimia* **1988**, *42*, 297. (f) Traldi, P.; Hamdan, M.; Paradisi, C. *J. Am. Chem. Soc.* **1990**, *112*, 4774.

(29) The ADF package is available from: te Velde, G.; Baerends, E. J., Department of Theoretical Chemistry, Vrije Universiteit, Amsterdam, The Netherlands.

(30) Snijders, J. G.; Baerends, E. J. *Mol. Phys.* **1977**, *33*, 1651.

(31) Vosko, S. H.; Wilk, L.; Nusair, M. *Can. J. Phys.* **1980**, *58*, 1200.

(32) Becke, A. D. *Phys. Rev. A* **1988**, *38*, 3098.

(33) Perdew, J. P. *Phys. Rev. B* **1986**, *33*, 8822.

(34) Levy, M.; Perdew, J. P. *Int. J. Quantum Chem.* **1994**, *49*, 539.

(35) (a) Werner, H.-J.; Knowles, P. J. *J. Chem. Phys.* **1985**, *82*, 5053. (b) Knowles, P. J.; Werner, H.-J. *Chem. Phys. Lett.* **1985**, *115*, 259.

(36) Werner, H.-J.; Knowles, P. J. *Theor. Chim Acta* **1990**, *78*, 175.

(37) MOLPRO96 is a package of ab initio programs written by H.-J. Werner and P. J. Knowles, with contributions from Almlöf, J.; Amos, R. D.; Deegan, M. J. O.; Elbert, S. T.; Hampel, C.; Meyer, W.; Peterson, K.; Pitzer, R.; Stone, A. J.; Taylor, P. R.; Lindh, R.

(38) Dolg, M.; Wedig, U.; Stoll, H.; Preuss, H. *J. Chem. Phys.* **1987**, *88*, 866.

(39) Woon, D. E., Dunning, T. H., Jr. *J. Chem. Phys.* **1993**, *98*, 1358.

(40) (a) Widmark, P.-O.; Malmquist, P.-A.; Roos, B. O. *Theor. Chim. Acta* **1990**, *77*, 291. (b) Pierloot, K.; Dunez, B.; Widmark, P.-O.; Roos, B. O. Unpublished results. (c) Pou-Amerigo, R.; Merchan, M.; Widmark, P.-O. Unpublished results.

(41) Pou-Amerigo, R.; Merchan, M.; Nebot-Gil, I.; Widmark, P.-O.; Roos, B. *Theor. Chim. Acta* **1995**, *92*, 149.

(42) Widmark, P.-O.; Persson, B. J.; Roos, B. O. *Theor. Chim. Acta* **1991**, *79*, 419.

(43) Woon, D. E.; Dunning, T. H., Jr. Unpublished results.

(44) Sievers, M. R.; Armentrout, P. B. *J. Chem. Phys.* **1995**, *102*, 754.

(45) Kappes, M. M.; Staley, R. H. *J. Phys. Chem.* **1981**, *85*, 942.

(46) At 10 eV, the $VO_2^+ + Xe$ reaction yields VO^+ (cross section of 1×10^{-16} cm^2) and V^+ (cross section $< 0.1 \times 10^{-16}$ cm^2). Rue, C.; Armentrout, P. B. Unpublished results.

(47) Results from the reactions of ScS^+, TiS^+, YS^+, ZrS^+, and NbS^+ with CO_2 (unpublished results) support the assignment of the small feature in the VS^+/CO_2 system to the S/O exchange process (16).

(48) VO_2^+ has a $^1A_1$ ground state; see: Harvey, J. N.; Diefenbach, M.; Schröder, D.; Schwarz, H. *Int. J. Mass Spectrom.*, submitted for publication.

(49) Density functional calculations on the B3LYP/6-311+G* level of theory reveal that the formation of CO ($^1\Sigma^-$) + S_2 ($^3\Sigma_g$) is favored over the formation of dithiacyclopropanone, OCS_2 ($^1A_1$), by 0.09 eV. Because B3LYP is known to underestimate the energies of the separated molecules (CO and S_2) with respect to the OCS_2 molecule, the theoretical data support the assignment of reaction 21 even more strongly.

(50) (a) Clemmer, D. E.; Aristov, N.; Armentrout, P. B. *J. Phys. Chem.* **1993**, *97*, 544. (b) Clemmer, D. E.; Chen, Y.-M.; Aristov, N.; Armentrout, P. B. *J. Phys. Chem.* **1994**, *98*, 7538.

(51) In the analogous reaction of VO^+ with D_2, Clemmer et al. have assigned the thresholds for formation of V^+ in excited states, predominantly the a^3F state as described in detail in ref 50a.

(52) Conceicao, J.; Loh, S. K.; Lian, L.; Armentrout, P. B. *J. Chem. Phys.* **1996**, *104*, 3976.

(53) Data below 1.5 eV is simply noise, which is larger for this channel because of its proximity in mass to the intense VS^+ beam.

(54) Bouchoux, G.; Salpin, J. Y.; Leblanc, D. *Int. J. Mass Spectrom. Ion Processes* **1996**, *153*, 37.

(55) (a) Dyke, J. M.; Gravenor, B. W. J.; Hastings, M. P.; Morris, A. *J. Phys. Chem.* **1985**, *89*, 4613. (b) Harrington, J.; Weisshaar, J. C. *J. Chem. Phys.* **1992**, *97*, 2809.

(56) Carter, E. A.; Goddard, W. A., III *J. Phys. Chem.* **1988**, *92*, 2109.

(57) Shaik, S.; Danovich, D.; Fiedler, A.; Schröder, D.; Schwarz, H. *Helv. Chim. Acta* **1995**, *78*, 1393.

(58) NBO Version 3.1, Glendening, E. D.; Reed, A. E.; Carpenter, J. E.; Weinhold, F. Gaussian, Inc.: Pittsburgh, PA, 1994.

(59) Clemmer, D. E.; Elkind, J. L.; Aristov, N.; Armentrout, P. B. *J. Chem. Phys.* **1991**, *95*, 3387.

(60) Hales, D. A.; Lian, L.; Armentrout, P. B. *Int. J. Mass Spectrom. Ion Processes* **1990**, *102*, 269.

(61) Hales, D. A.; Armentrout, P. B. *J. Cluster Sci.* **1990**, *1*, 127.

(62) Sievers, M. R.; Armentrout, P. B. *J. Phys. Chem.* **1995**, *99*, 8135.

(63) Aristov, N.; Armentrout, P. B. *J. Phys. Chem.* **1986**, *90*, 5135.

(64) Sievers, M. R.; Chen, Y.-M.; Armentrout, P. B. *J. Chem. Phys.* **1996**, *105*, 6322.

(65) Elkind, J. L.; Armentrout, P. B. *J. Phys. Chem.* **1985**, *89*, 5626.

(66) (a) Saillard, Y.; Grandjean, D.; Caillet, P.; Le Beuze, A. *J. Organomet. Chem.* **1975**, *94*, 409. (b) Andrews, M. A. *Inorg. Chem.* **1977**, *16*, 497.

(67) Werner, H. *Angew. Chem., Int. Ed. Engl.* **1990**, *29*, 1077.

(68) Jeung, G.-H. *J. Am. Chem. Soc.* **1992**, *114*, 3211.

(69) Kretzschmar, I.; Schwarz, H. Unpublished results.

(70) (a) Tilson, J. L.; Harrison, J. F. *J. Phys. Chem.* **1991**, *95*, 5097. (b) Tilson, J. L.; Harrison, J. F. *J. Phys. Chem.* **1992**, *96*, 1667.

(71) For a similar situation in $MnOH^+$, see: Ryan, M. F.; Fiedler, A.; Schröder, D.; Schwarz, H. *J. Am. Chem. Soc.* **1995**, *117*, 2033.

(72) (a) For $ScOH^+$, see: Bauschlicher, C. W., Jr.; Patridge, H. *Chem Phys. Lett.* **1997**, *272*, 127. (b) For $TiOH^+$, see: Irigoras, A.; Fowler, J. E.; Ugalde, J. M. *J. Phys. Chem. A* **1998**, *102*, 293.

(73) Taylor, J. R. *An Introduction to Error Analysis*; University Science Books: Mill Valley, CO, 1982.

(74) For the VS^+ ($^3\Sigma^-$) ground state, spin−orbit coupling can be neglected, while that for V^+ (^{5}D) amounts to 0.02 eV.

(75) (a) For a review about BSSE, see: van Duijneveldt, F. B.; van Duijneveldt-van de Rijdt, J. G. C. M.; van Lenthe, J. *Chem. Rev.* **1970**, *19*, 553. (b) See also: Jensen, F. *Chem. Phys. Lett.* **1997**, *280*, 381.

(76) (a) Bauschlicher, C. W., Jr.; Maitre, P. *Theor. Chim. Acta* **1995**, *90*, 189. (b) See also: Bauschlicher, C. W., Jr.; Langhoff, S. R. *J. Chem. Phys.* **1986**, *85*, 5935.

(77) Huber, K. P.; Herzberg, G. *Constants of Diatomic Molecules*; Van Nostrand Reinhold: New York, 1979.

(78) (a) Fiedler. A.; Schröder, D.; Shaik, S.; Schwarz, H. *J. Am. Chem. Soc.* **1994**, *116*, 10734. (b) Shaik, S.; Filatov, M.; Schröder, D.; Schwarz, H. *Chem. Eur. J.* **1998**, *4*, 193.

(79) For TSR in organic ions, see: (a) Aschi, M.; Harvey, J. N.; Schalley, C. A.; Schröder, D.; Schwarz, H. *J. Chem. Soc., Chem. Commun.* **1998**, 531. (b) Schröder, D.; Heinemann, H.; Schwarz, H.; Harvey, J. N.; Dua, S.; Blansky, S. J.; Bowie, J. H. *Chem. Eur. J.*, in press.